Biotinylated cTnC was immobilized on the avidin-coated QCM Au electrode and the sensor tips were immersed in a solution consisting of (in mM) 43 MOPS/KOH (pH 7.0), 500 KCl, 0.9 $MgCl_2$ and 3.5 EGTA. Binding of the cTnI N-terminal peptide to cTnC were detected from ΔF upon cumulative injection of cTnI N-terminal peptide into the bathing solution. High ionic strength conditions were adopted to reduce non-specific binding of the N-terminal peptide to electrodes.

Generation of a transgenic mouse model of HCM

Cloning and mutagenesis of human cTnT cDNA were carried out as described previously (Morimoto *et al.*, 1998; 2002). About 1.3 kb of the upstream promoter region of the mouse cTnT gene obtained from genomic mouse DNA by PCR was replaced into an MHC class I promoter fragment of the cDNA expression vector pLG1 (Morimoto *et al.*, 2002), and designated as pTG. The recombinant cDNA encoding the WT or ΔE160 mutant cTnT was introduced into the cDNA cloning site of the plasmid pTG. The SpeI-XhoI fragment isolated as a transgene was then microinjected into the pronucleus of fertilized eggs of C57BL/6 mice. Identification of the transgene in founder mice and their progeny was performed by Southern blot analysis and PCR using genomic DNA isolated from tail. Homozygous transgenic mice were produced by mating between heterozygous ΔE160 cTnT transgenic mice and were used in this study. Homozygosity was determined by genotyping using PCR. Human cTnT transgene mRNA expression was detected by RT-PCR using a set of primers (5′-ACC ACC TTC TGA TAG GCA G and 5′-TCT GAC ATA GAA GAG GTG GTG), which amplify a 902 bp DNA fragment. Expression level of the cTnT transgene protein was determined by immunoblot analyses of the skinned cardiac muscle fibres using the monoclonal anti-human cTnT antibody 2D10 (Research Diagnostic, Concord, MA, USA), which does not react with mouse cTnT and the monoclonal anti-TnT antibody JLT-12 (Oncogene Science, Cambridge, MA, USA), which cross-reacts with human and mouse cTnTs equally. The transgenic mice were fed with standard rodent chow and water provided *ad libitum*.

Analysis of working isolated hearts

Hearts were excised from mice after anaesthesia with pentobarbital sodium (50 $mg \cdot kg^{-1}$, i.p.) and heparinization (15 U i.v.). The working hearts were prepared and analysis was carried out as described previously (Mizukami *et al.*, 2008).

Measurements of Ca^{2+} transient in isolated cardiomyocytes

Cardiomyocytes isolated from mouse left ventricle were loaded with Fura-2 acetoxymethyl ester, and $[Ca^{2+}]_i$ was monitored using a fluorescence recording system (IonOptix LLC, Milton, MA, USA) as described previously (Du *et al.*, 2007).

Data analysis

Data are presented as mean ± SEM. Mean values for more than three groups were compared by one-way analysis of variance, followed by a *post hoc* Dunnett's or Tukey's multiple comparison test. The difference between two group means was analysed with an unpaired Student's *t*-test.

Materials

Catechins were purchased from Wako Pure Chemical Industries, Ltd. (Osaka, Japan).

Results

Figure 1 shows the structures of catechins examined in this study. Figure 2A shows the force-pCa relationships in skinned cardiac muscle fibres determined in the presence of epicatechin derivatives EC, EGC, ECg and EGCg. ECg and EGCg were found to decrease Ca^{2+} sensitivity, as shown by rightward shifts of the force-pCa relationships with significant reduction in pCa_{50}. EGCg had a greater Ca^{2+}-desensitizing effect than ECg. EC and EGC had no significant effects on cardiac myofilament Ca^{2+}-sensitivity, indicating that the galloyl group in ECg and EGCg has a critical role in the Ca^{2+}-desensitizing effects. On the other hand, closely related catechin compounds, including (-)-catechin-3-gallate and (-)-gallocatechin-3-gallate, which are diastereomers of ECg and EGCg, respectively, had no significant effects on the Ca^{2+} sensitivity of skinned cardiac muscle fibres (Figure 2B), strongly suggesting that Ca^{2+}-desensitizing effects of ECg and EGCg derived from a specific stereoselective molecular interaction with a target molecule in cardiac muscle. These epicatechin and catechin derivatives had no significant effects on the maximum force in skinned cardiac muscle fibres (data not shown). EGCg decreased the Ca^{2+} sensitivity of skinned cardiac muscle fibres in a concentration-dependent manner (Figure 2C).

EGCg was found to have a much weaker effect on the Ca^{2+} sensitivity of fast skeletal muscle compared with cardiac muscle (Figure 3A). Because cardiac and fast skeletal muscle contraction is regulated by specific isoforms of Tn, cTn and fsTn, respectively, we tested the possibility that the cardiac isoform of Tn

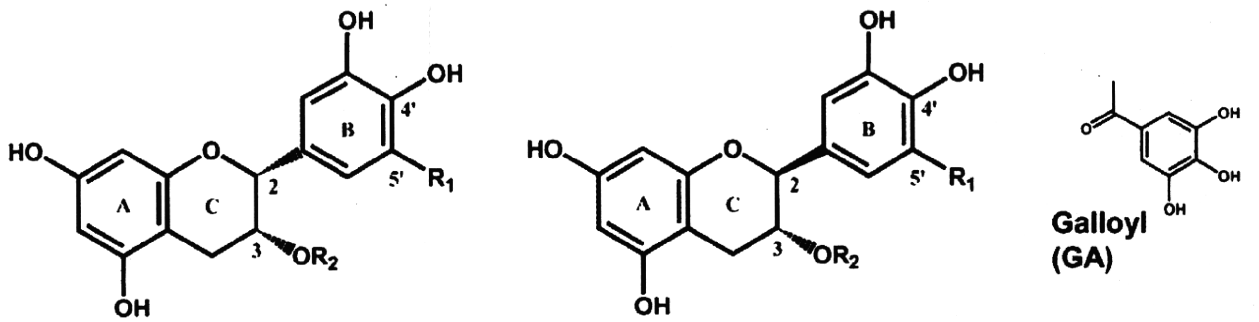

	R_1	R_2
(-)-Epicatechin (EC)	H	H
(-)-Epigallocatechin (EGC)	OH	H
(-)-Epicatechin gallate (ECg)	H	GA
(-)-Epigallocatechin gallate (EGCg)	OH	GA
(-)-Catechin (C)	H	H
(-)-Gallocatechin (GC)	OH	H
(-)-Catechin gallate (Cg)	H	GA
(-)-Gallocatechin gallate (GCg)	OH	GA

Figure 1

The structures of epicatechin and catechin derivatives used in this study.

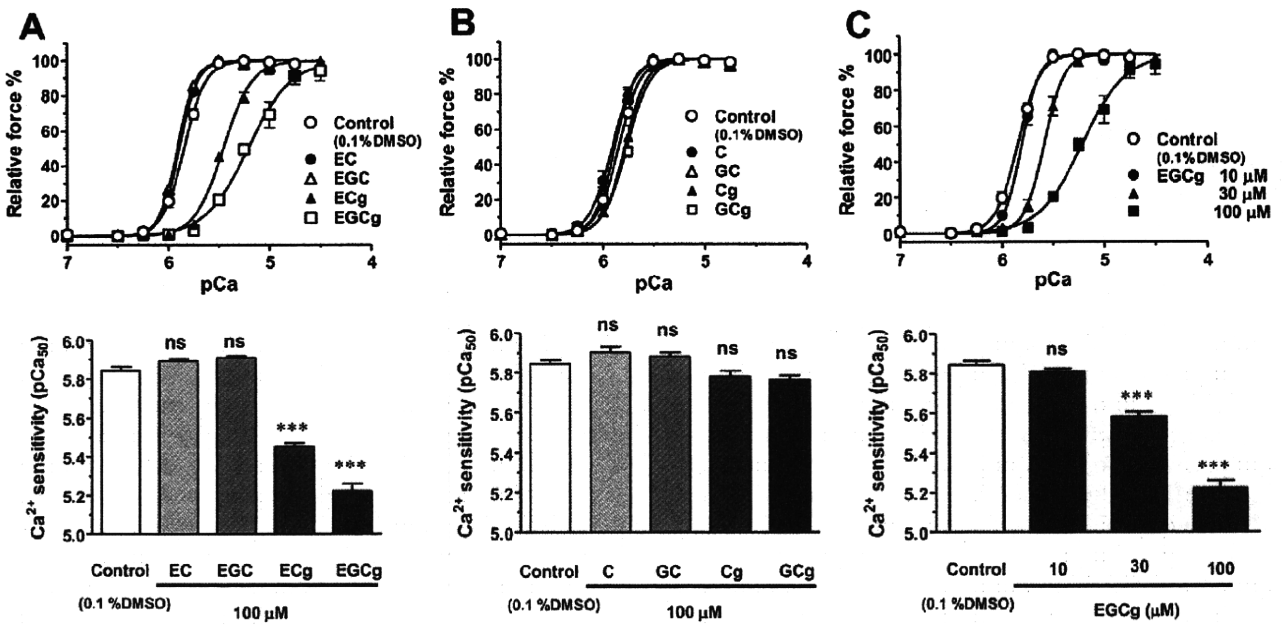

Figure 2

Effects of catechins on force generation in skinned cardiac muscle fibres. (A) Upper panel: Force-pCa relationships determined in the presence of 100 μM epicatechin derivatives. Lower panel: Effects of epicatechin derivatives on the Ca^{2+} sensitivity (pCa_{50}) of force generation in skinned cardiac muscle fibres. (B) Upper panel: Force-pCa relationships determined in the presence of 100 μM catechin derivatives. Lower panel: Effects of catechin derivatives on the Ca^{2+} sensitivity (pCa_{50}) of force generation in skinned cardiac muscle fibres. (C) Upper panel: Force-pCa relationships in skinned cardiac muscle fibres determined in the presence of 10, 30 and 100 μM EGCg. Lower panel: Concentration-dependent effects of EGCg on the Ca^{2+} sensitivity (pCa_{50}) of force generation in skinned cardiac muscle fibres. The data represent the means ± SE of measurements on 10 and 5 fibres for control and samples, respectively. ***$P < 0.001$ versus control (Dunnett's multiple comparison test). C, catechin; Cg, (-)-catechin-3-gallate; EC, (-)-Epicatechin; ECg, (-)-Epicatechin-3-gallate; EGC, (-)-Epigallocatechin; EGCg, (-)-Epigallocatechin-3-gallate; GC, gallocatechin; GCg, (-)-gallocatechin-3-gallate.

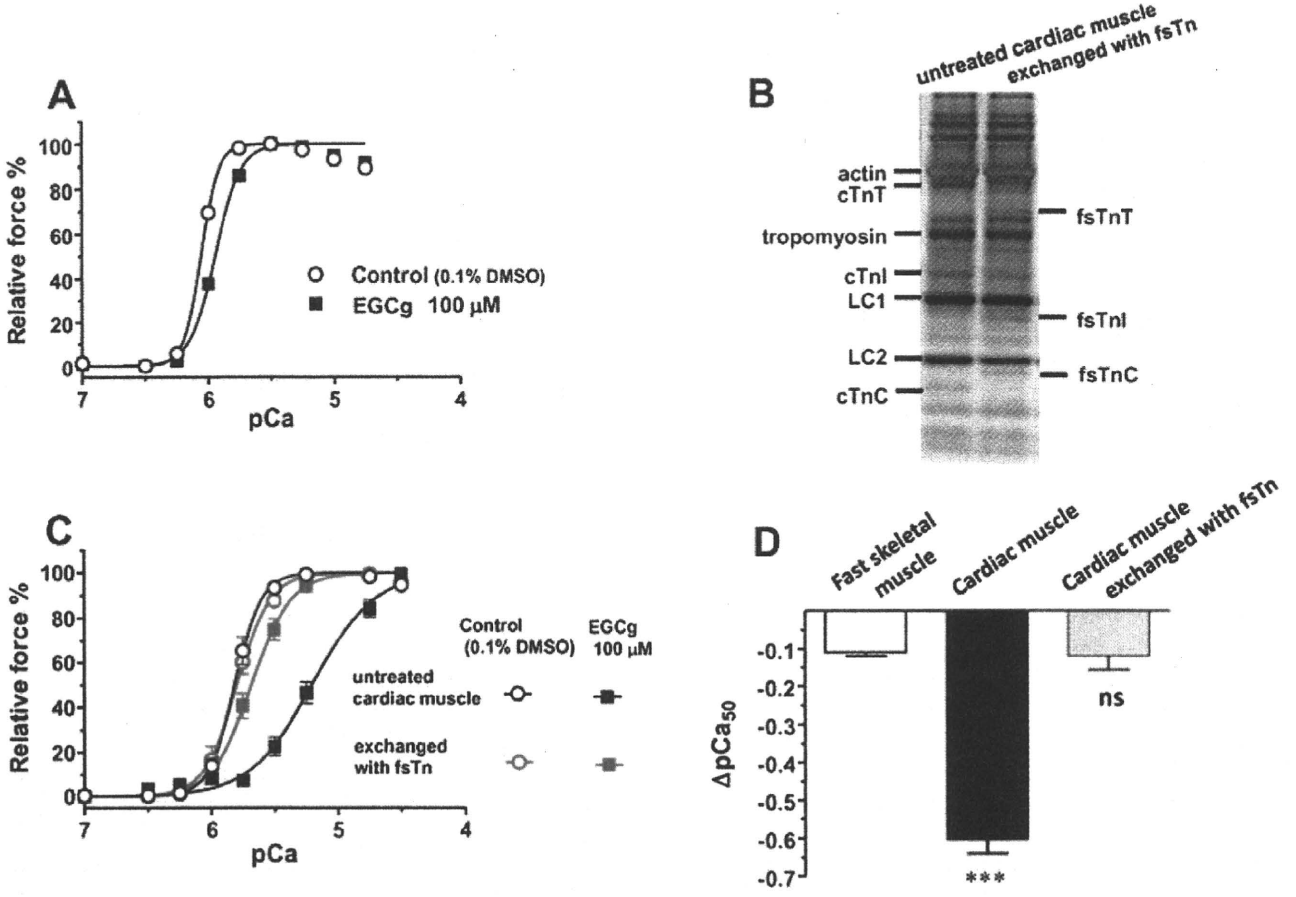

Figure 3

Role of Tn in determining the differential sensitivity to EGCg in cardiac and fast skeletal muscle. (A) Effect of EGCg on force-pCa relationships in skinned fast skeletal muscle fibres. The data represent the means ± SE of measurements on 5 fibres. (B) SDS-PAGE analysis of skinned cardiac muscle fibres in which endogenous cTn was exchanged with fsTn. Note that the decrease in cTnI was not apparent due to the presence of other protein(s) with similar mobility. Densitometric analyses of TnC isoforms in skinned fibres indicated that 83.5 ± 3.0% ($n = 7$ fibres) of endogenous Tn was exchanged with fsTn. LC1 and LC2, ventricular myosin light chains 1 and 2, respectively. (C) Effect of EGCg on force-pCa relationships in skinned cardiac muscle fibres exchanged with fsTn. The data represent the means ± SE of measurements on 7 fibres. (D) EGCg-induced decrease in the Ca^{2+}-sensitivity (ΔpCa_{50}) in skinned cardiac muscle fibres exchanged with fsTn. The data represent the means ± SE of measurements on 7 fibres. ***$P < 0.001$ versus fast skeletal muscle (Dunnett's multiple comparison test). EGCg, (-)-Epigallocatechin-3-gallate; fsTn, fast skeletal muscle troponin; Tn, troponin.

might be responsible for the greater effect of EGCg on cardiac muscle, by exchanging whole Tn complex in skinned fibres (Figure 3B). Exchanging endogenous cTn in skinned cardiac muscle fibres with fsTn reduced the Ca^{2+}-desensitizing effect of EGCg to almost the same level as that observed in the fast skeletal muscle fibres (Figures 3C,D). These results provide strong evidence that cTn is a specific target of EGCg in cardiac muscle that determines the greater effect of EGCg on the Ca^{2+} sensitivity of cardiac muscle, compared with its effects on fast skeletal muscle.

We next measured the binding of EGCg to the cTn subunits, using a quartz crystal microbalance (QCM), a very sensitive mass measuring device. QCM analyses indicated that EGCg bound to cTnC, but not to cTnI or cTnT (Figure 4A). Using nuclear magnetic resonance (NMR) spectroscopy, we have previously demonstrated that EGCg bound to the C-lobe of cTnC (Tadano *et al.*, 2005a,b). As the C-lobe of cTnC is known to interact with an N-terminal α-helical region of cTnI, we measured the binding of the N-terminal peptide of cTnI ($cTnI_{35-62}$) to cTnC, in the absence and presence of EGCg (Figure 4B). The results indicated that EGCg enhanced the binding of the N-terminal H1 helix region of cTnI to cTnC.

Mutations in genes of human cTn subunits have been found to cause HCM (Harada and Morimoto, 2004; Marian, 2005). *In vitro* and *in vivo* studies

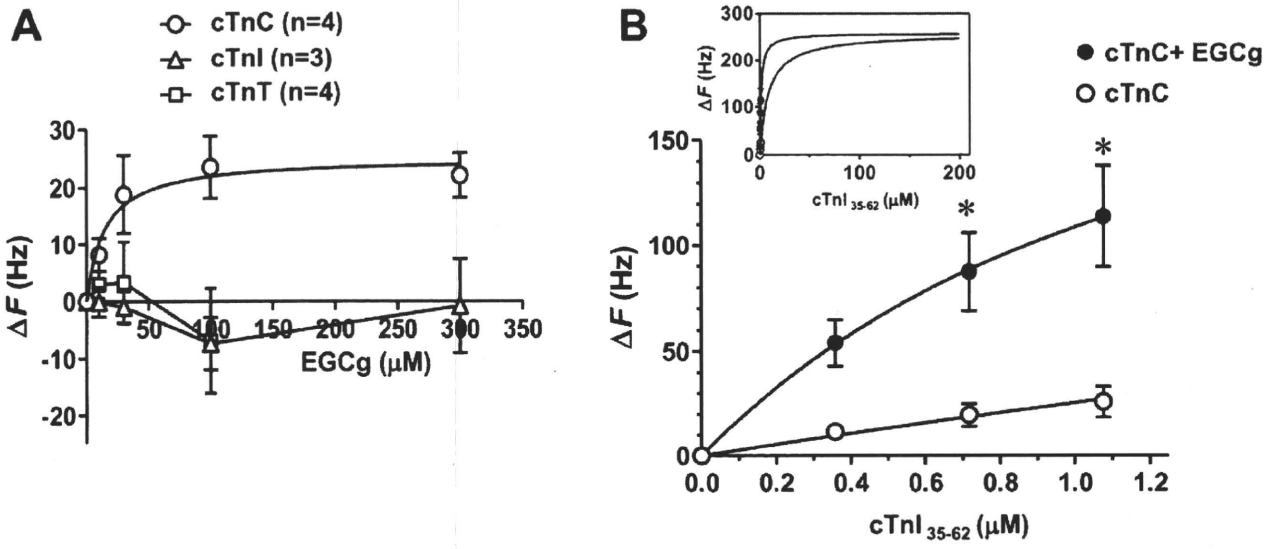

Figure 4

Binding of EGCg to cTn subunits. (A) Binding of EGCg to cTnC, cTnI and cTnT were directly determined from the frequency changes (ΔF) of QCM upon cumulative addition of EGCg. The data represent the means ± SE of 3–4 measurements. The EGCg-cTnC binding data were fitted to a hyperbolic one-site binding equation, and a best-fitted curve was obtained with a K_D of 14.6 μM. (B) Effects of EGCg on the binding of a cTnI N-terminal peptide ($cTnI_{35-62}$) to cTnC. Binding of the cTnI N-terminal peptide ($cTnI_{35-62}$) to cTnC was directly determined from ΔF of QCM upon cumulative addition of the peptide in the absence or presence of 300 μM EGCg. The data represent the means ± SE of 3 measurements. *$P < 0.05$, versus –EGCg (unpaired *t*-test). The data were fitted to a hyperbolic one-site binding equation, and best-fitted curves were obtained with K_D's of 9.1 and 1.4 μM for cTnC and cTnC+EGCg, respectively. EGCg, (-)-Epigallocatechin-3-gallate; QCM, quartz crystal microbalance.

using mutant proteins and transgenic animals indicate that an increased Ca^{2+} sensitivity of cardiac myofilament is the causal functional defect triggering the pathogenesis of HCM associated with the mutations in cTn subunits (Harada and Morimoto, 2004; Ahmad *et al.*, 2005; Morimoto, 2008; Morimoto, 2009). We created a transgenic mouse model of HCM expressing the deletion mutant ΔE160 of cTnT in the heart, which had been found to cause familial HCM in human (Figures 5A–C). The mutant mice showed extensive level of cardiomyocyte disarray (Figure 5D), a hallmark of HCM, and Ca^{2+}-sensitization in the force generation of skinned cardiac muscle fibres (Figure 5E). EGCg reversed the increased myofilament Ca^{2+} sensitivity of mutant mice (Figure 5E). *Ex vivo* analyses of isolated working heart preparations showed normal systolic function with diastolic dysfunction, another hallmark of HCM, as shown by preserved left ventricular dP/dt_{max} and decreased left ventricular $-dP/dt_{min}$ (Figure 6A). Cardiac output from the hearts of ΔE160cTnT-Tg mice was significantly lower than those from WTcTnT-Tg mice or Non-Tg mice due to diastolic dysfunction (Figure 6B). EGCg improved the diastolic dysfunction of the hearts of these mice (Figure 6A) and increased their cardiac output (Figure 6B). EGC had no such beneficial effects on the diastolic function and cardiac output (data not shown). Figure 6C shows Ca^{2+} transients measured in Fura-2-loaded cardiomyocytes. The peak amplitude and the peak rates of increase and decrease in cytoplasmic Ca^{2+} were decreased in ΔE160cTnT-Tg mice as in the other Tg mouse models of HCM caused by mutations of cTnI and cTnT (Wen *et al.*, 2008; Willott *et al.*, 2010); EGCg tended to restore these parameters of Ca^{2+} transient. The resting Ca^{2+} levels of ΔE160cTnT-Tg mice were not significantly different from those of WTcTnT-Tg mice; EGCg had no significant effects on the resting Ca^{2+} levels.

Discussion

In this study, we found that ECg and EGCg, major polyphenols in green tea, are Ca^{2+} desensitizers that directly decrease the Ca^{2+} sensitivity of cardiac myofilaments. We have previously reported that EGCg induced amide chemical shift perturbations on several residues of cTnC in NMR spectroscopy (Figure S1) (Tadano *et al.*, 2005a,b). The residues T124, G125 and I128 of the FG loop and the C-terminal residue E161 in the C-lobe undergo significant chemical shift perturbations. GCg, a diastereomer of EGCg, did not induce the chemical shift perturbations on these residues of cTnC (data not shown).

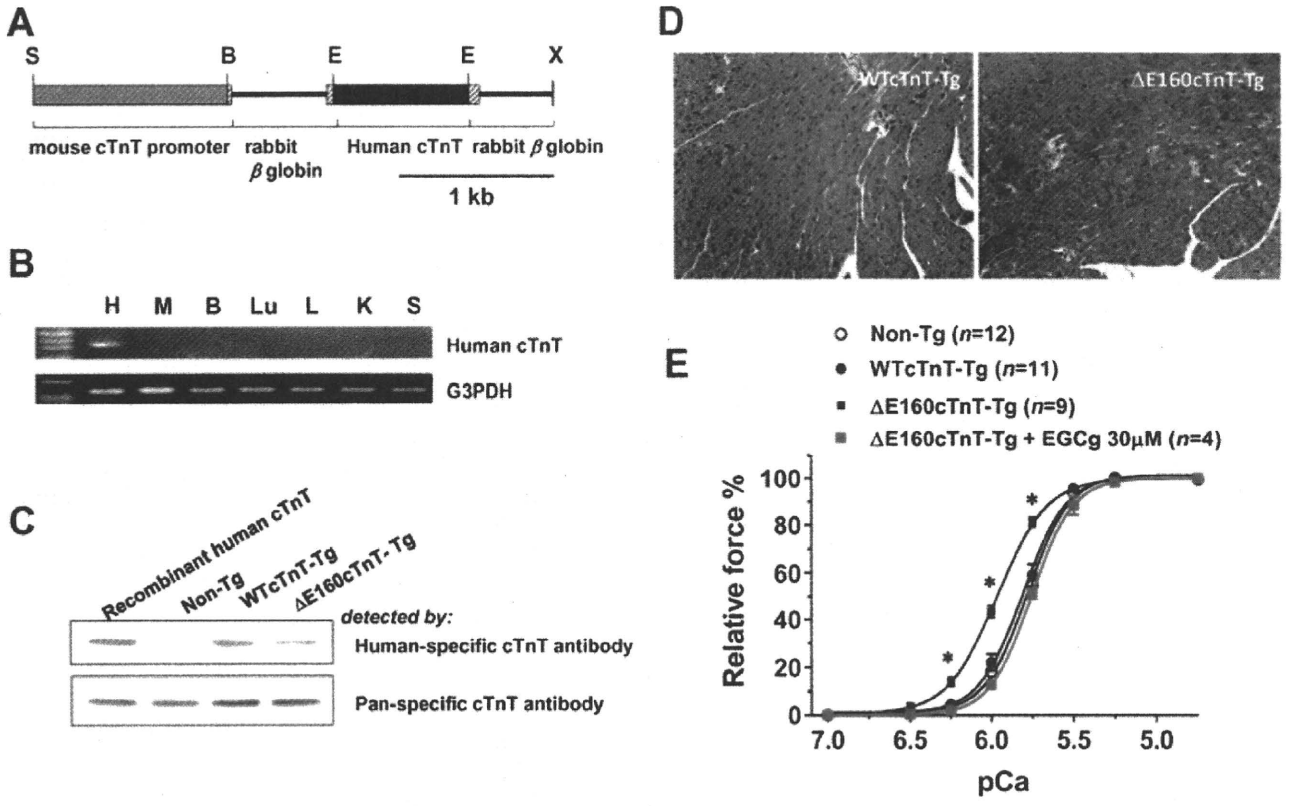

Figure 5

Creation of a transgenic mice model for hypertrophic cardiomyopathy. (A) The transgene used to generate the transgenic mice expressing the ΔE160 mutant cTnT. S, *SpeI*; B, *BamHI*; E, *EcoRI*; X, *XhoI*. (B) RT-PCR analysis of total RNA extracted from various tissues (H, heart; M, skeletal muscle; B, brain; Lu, lung; L, liver; K, kidney; S, spleen) demonstrating heart-specific expression of the transgene. (C) Immunoblot analyses of the skinned cardiac muscle fibres. Human cTnT and total cTnT were detected using a monoclonal anti-human cTnT specific antibody (upper panel) and a monoclonal anti-pan specific TnT antibody (lower panel), respectively. Expression levels of human cTnT in WTcTnT-Tg and ΔE160cTnT-Tg mice were about 60 and 30%, respectively, as determined by using the density ratio of human cTnT to total cTnT for purified human cTnT as 100%. (D) Histology of hearts (HE staining) excised from 3 months old anesthetized Tg mice. (E) Force-pCa relationships in the skinned cardiac muscle fibres. The data represent the means ± SE of measurements on *n* fibers from different mice. $*P < 0.05$ versus non- or WTcTnT-Tg mice (Tukey's multiple comparison test).

These results strongly suggest that EGCg binds to a region near the FG loop in the C-lobe, consistent with a recent NMR spectroscopic study using a C-terminal half peptide of cTnC (Robertson *et al.*, 2009), and also binds to a region near the C-terminus of cTnC in a stereospecific manner, both of which lie in a close vicinity to the binding site of the N-terminal H1 helix (residues 43–79) of cTnI (Figure S2). The present study, together with these previous NMR spectroscopic studies, strongly suggest that EGCg causes a Ca^{2+}-desensitization of cardiac myofilaments by enhancing the interaction of the H1 helix of cTnI with the C-lobe of cTnC through its stereospecific binding to the C-termininal regions of cTnC. Interestingly, a Ca^{2+} sensitizer EMD57033, which directly increases the Ca^{2+} sensitivity of cardiac myofilament, has been reported to disrupt the interaction of the N-terminal helix region of cTnI with the C-lobe of cTnC (Wang *et al.*, 2001), strongly suggesting that the stability of this interaction plays a critical role in determining the Ca^{2+} sensitivity of cardiac myofilaments.

A recent NMR spectroscopic study has reported that EGCg binds to the C-terminal half peptide of cTnC very weakly with a K_D of 0.4–1 mM (Robertson *et al.*, 2009). However, aromatic stacking of EGCg occurs in aqueous solution at high concentrations of EGCg (Kitano *et al.*, 1997; Wroblewski *et al.*, 2001), and this additional equilibrium would confound accurate K_D determination in NMR spectroscopy (Robertson *et al.*, 2009). In fact, a fluorescence spectroscopic study using low concentrations of EGCg shows that EGCg strongly binds to cTnC with a K_D of 3–4 μM (Liou *et al.*, 2008). The present QCM study also shows that EGCg binds to cTnC with a high affinity (K_D value 15 μM). A significant

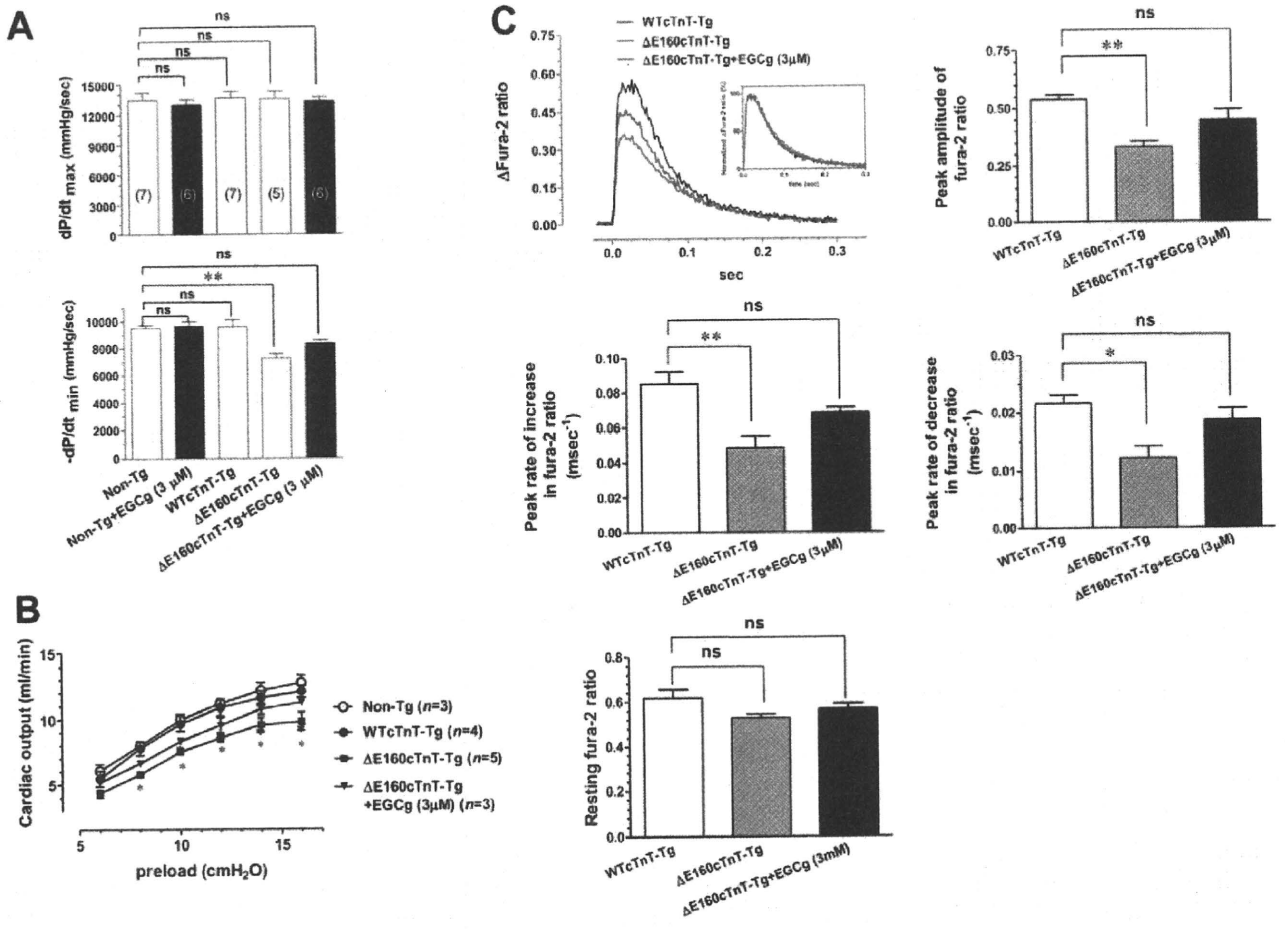

Figure 6

Effects of EGCg on cardiac muscle function of HCM mice. (A) Maximum and minimum derivatives of left ventricular pressure determined on working heart preparations. The data represent the means ± SE for the numbers of hearts indicated in parentheses. (B) Cardiac outputs from isolated working hearts of 2–3 months old mice. The data represent the means ± SE of *n* hearts. (C) Ca^{2+} transients induced by electrical stimulation at 3 Hz in left ventricular cardiomyocytes. The data represent the means ± SE of parameters determined on nine cardiomyocytes from three3 hearts. $^{**}P < 0.01$ versus non-Tg mice in panel A; $^{*}P < 0.05$, $^{**}P < 0.01$ versus WTcTnT-Tg mice in panels B and C (Dunnett's multiple comparison test). EGCg, (-)-Epigallocatechin-3-gallate; HCM, hypertrophic cardiomyopathy.

Ca^{2+}-desensitizing effect of EGCg, however, was only detected at above 30 μM on the skinned cardiac muscle fibres. Although the reason for this discrepancy remains to be elucidated, it should be noted that the effective concentrations of Ca^{2+}-sensitizers pimobendan and EMD57033 in skinned cardiac muscle fibres were also reported to be much higher than those estimated *in vivo* (Fujino *et al.*, 1988; Solaro *et al.*, 1993; Chu *et al.*, 1999), suggesting that drugs generally have much lower potency in skinned cardiac muscle preparations than *in vivo*. In the present study, a low concentration of EGCg (3 μM) improved the diastolic dysfunction of the hearts of ΔE160cTnT-Tg mice and increased their cardiac output. We found that the peak amplitude and the peak rates of increase and decrease in cytoplasmic Ca^{2+} were significantly decreased in the cardiomyocytes of ΔE160cTnT-Tg mice, irrespective of the fact that the hearts of these mice showed no significantly altered myocardial contractility assessed by the left ventricular dP/dt_{max}. These findings suggest that sarcoplasmic reticulum (SR) function in ΔE160cTnT-Tg mice might be reduced to suppress an enhanced contractility expected to be caused by increased myofilament Ca^{2+} sensitivity at the cost of retardation of relaxation, in an opposite manner to the case we have demonstrated in a mouse model of dilated cardiomyopathy caused by decreased myofilament Ca^{2+} sensitivity (Du *et al.*, 2007). We also found that EGCg increased the Ca^{2+} transient in ΔE160cTnT-Tg mice without changing the myocardial contractility assessed by the left ventricular dP/dt_{max} and improved the diastolic dysfunction without changing the resting Ca^{2+} level.

These results suggest that EGCg restores the impaired cardiac pump function due to diastolic dysfunction by reversing the increased Ca^{2+} sensitivity of cardiac myofilaments. Although further studies are needed to see if EGCg has any direct effect on SR function, the enhancement of Ca^{2+} transients by EGCg should be at least partly due to a decrease in sarcomeric Ca^{2+} buffering that could be caused by Ca^{2+} desensitizing effect of EGCg on cTnC.

HCM is an inherited cardiac disease with a high prevalence and is the main cause of sudden death of young adults, with no therapy being currently established. Many mutations in genes for sarcomeric proteins have been found to cause HCM (Harada and Morimoto, 2004; Marian, 2005), and increased Ca^{2+} sensitivity of cardiac myofilaments is found to be a primary cause for the pathogenesis of HCM, at least those forms associated with the mutations in the regulatory proteins cTnT, cTnI, cTnC and α-tropomyosin (Ahmad *et al.*, 2005). To our knowledge, EGCg and ECg are the first chemical compounds that could ameliorate diastolic dysfunction of HCM, at least partially, through their direct Ca^{2+}-desensitizing effects on cardiac myofilament. The present study suggests that EGCg or ECg might be a useful material or lead compound for development of therapeutic agents to treat the inherited HCM caused by increased myofilament Ca^{2+} sensitivity.

Acknowledgements

This work was supported in part by Grants-in-Aid, Special Coordination Funds and National Project on Protein Structural and Functional Analyses for Scientific Research from the Ministry of Education, Culture, Sports, Science and Technology of Japan.

Conflict of interest

None declared.

References

Ahmad F, Seidman JG, Seidman CE (2005). The genetic basis for cardiac remodeling. Annu Rev Genomics Hum Genet 6: 185–216.

Arts IC, Hollman PC, Feskens EJ, Bueno de Mesquita HB, Kromhout D (2001). Catechin intake might explain the inverse relation between tea consumption and ischemic heart disease: the Zutphen Elderly Study. Am J Clin Nutr 74: 227–232.

Chu K-M, Hu OY-P, Shieh S-M (1999). Cardiovascular effect and simultaneous pharmacokinetic and pharmacodynamic modeling of pimobendan in healthy normal subjects. Drug Metab Dispos 27: 701–709.

Chyu KY, Babbidge SM, Zhao X, Dandillaya R, Rietveld AG, Yano J *et al.* (2004). Differential effects of green tea-derived catechin on developing versus established atherosclerosis in apolipoprotein E-null mice. Circulation 109: 2448–2453.

Du CK, Morimoto S, Nishii K, Minakami R, Ohta M, Tadano N *et al.* (2007). Knock-in mouse model of dilated cardiomyopathy caused by troponin mutation. Circ Res 101: 185–194.

Fujino K, Sperelakis N, Solaro R (1988). Sensitization of dog and guinea pig heart myofilaments to Ca^{2+} activation and the inotropic effect of pimobendan: comparison with milrinone. Circ Res 63: 911–922.

Harada K, Morimoto S (2004). Inherited cardiomyopathies as a troponin disease. Jpn J Physiol 54: 307–318.

Kitano K, Nam KY, Kimura S, Fujiki H, Imanishi Y (1997). Sealing effects of (-)-epigallocatechin gallate on protein kinase C and protein phosphatase 2A. Biophys Chem 65: 157–164.

Liou YM, Kuo SC, Hsieh SR (2008). Differential effects of a green tea-derived polyphenol (-)-epigallocatechin-3-gallate on the acidosis-induced decrease in the Ca^{2+} sensitivity of cardiac and skeletal muscle. Pflugers Arch 456: 787–800.

Lorenz M, Wessler S, Follmann E, Michaelis W, Dusterhoft T, Baumann G *et al.* (2004). A constituent of green tea, epigallocatechin-3-gallate, activates endothelial nitric oxide synthase by a phosphatidylinositol-3-OH-kinase-, cAMP-dependent protein kinase-, and Akt-dependent pathway and leads to endothelial-dependent vasorelaxation. J Biol Chem 279: 6190–6195.

Lu QW, Morimoto S, Harada K, Du CK, Takahashi-Yanaga F, Miwa Y *et al.* (2003). Cardiac troponin T R141W mutation found in dilated cardiomyopathy stabilizes the troponin T-tropomyosin interaction and causes a Ca^{2+} desensitization. J Mol Cell Cardiol 35: 1421–1427.

Ludwig A, Lorenz M, Grimbo N, Steinle F, Meiners S, Bartsch C *et al.* (2004). The tea flavonoid epigallocatechin-3-gallate reduces cytokine-induced VCAM-1 expression and monocyte adhesion to endothelial cells. Biochem Biophys Res Commun 316: 659–665.

Marian AJ (2005). Clinical and molecular genetic aspects of hypertrophic cardiomyopathy. Curr Cardiol Rev 1: 53–63.

Mirza M, Marston S, Willott R, Ashley C, Mogensen J, McKenna W *et al.* (2005). Dilated cardiomyopathy mutations in three thin filament regulatory proteins result in a common functional phenotype. J Biol Chem 280: 28498–28506.

Mizukami Y, Ono K, Du CK, Aki T, Hatano N, Okamoto Y *et al.* (2008). Identification and physiological activity of survival factor released from cardiomyocytes during ischaemia and reperfusion. Cardiovasc Res 79: 589–599.

Morimoto S (2008). Sarcomeric proteins and inherited cardiomyopathies. Cardiovasc Res 77: 659–666.

Morimoto S (2009). Expanded spectrum of gene causing both hypertrophic cardiomyopathy and dilated cardiomyopathy. Circ Res 105: 313–315.

Morimoto S, Yanaga F, Minakami R, Ohtsuki I (1998). Ca^{2+}-sensitizing effects of the mutations at Ile-79 and Arg-92 of troponin T in hypertrophic cardiomyopathy. Am J Physiol 275: C200–C207.

Morimoto S, Lu QW, Harada K, Takahashi-Yanaga F, Minakami R, Ohta M *et al.* (2002). Ca^{2+}-desensitizing effect of a deletion mutation Delta K210 in cardiac troponin T that causes familial dilated cardiomyopathy. Proc Natl Acad Sci USA 99: 913–918.

Mukamal KJ, Maclure M, Muller JE, Sherwood JB, Mittleman MA (2002). Tea consumption and mortality after acute myocardial infarction. Circulation 105: 2476–2481.

Okahata Y, Kawase M, Niikura K, Ohtake F, Furusawa H, Ebara Y (1998a). Kinetic measurements of DNA hybridization on an oligonucleotide-immobilized 27-MHz quartz crystal microbalance. Anal Chem 70: 1288–1296.

Okahata Y, Niikura K, Sugiura Y, Sawada M, Morii T (1998b). Kinetic studies of sequence-specific binding of GCN4-bZIP peptides to DNA strands immobilized on a 27-MHz quartz-crystal microbalance. Biochemistry 37: 5666–5672.

Robertson IM, Li MX, Sykes BD (2009). Solution structure of human cardiac troponin C in complex with the green tea polyphenol, (-)-epigallocatechin 3-gallate. J Biol Chem 284: 23012–23023.

Sasazuki S, Inoue M, Miura T, Iwasaki M, Tsugane S (2008). Plasma tea polyphenols and gastric cancer risk: a case-control study nested in a large population-based prospective study in Japan. Cancer Epidemiol Biomarkers Prev 17: 343–351.

Solaro R, Gambassi G, Warshaw D, Keller M, Spurgeon H, Beier N *et al.* (1993). Stereoselective actions of thiadiazinones on canine cardiac myocytes and myofilaments. Circ Res 73: 981–990.

Tachibana H, Koga K, Fujimura Y, Yamada K (2004). A receptor for green tea polyphenol EGCG. Nat Struct Mol Biol 11: 380–381.

Tadano N, Morimoto S, Sasaguri T (2005a). EGCg, a major polyphenol in green tea, binds to cardiac troponin C and desensitizes cardiac muscle contraction to Ca^{2+}. J Pharmacol Sci 97: 180P–180P.

Tadano N, Yumoto F, Tanokura M, Ohtsuki I, Morimoto S (2005b). EGCg, a major polyphenol in green tea, binds to the C-lobe of cardiac troponin and desensitizes cardiac muscle contraction to Ca^{2+}. Biophys J 88: 314a–314a.

Van Selst M, Jolicoeur P (1994). A solution to the effect of sample size on outlier elimination. Q J Exp Psychol A 47: 631–650.

Wang ZY, Wang LD, Lee MJ, Ho CT, Huang MT, Conney AH *et al.* (1995). Inhibition of N-nitrosomethylbenzylamine-induced esophageal tumorigenesis in rats by green and black tea. Carcinogenesis 16: 2143–2148.

Wang X, Li MX, Spyracopoulos L, Beier N, Chandra M, Solaro RJ *et al.* (2001). Structure of the C-domain of human cardiac troponin C in complex with the Ca^{2+} sensitizing drug EMD 57033. J Biol Chem 276: 25456–25466.

Wen Y, Pinto JR, Gomes AV, Xu Y, Wang Y, Potter JD *et al.* (2008). Functional consequences of the human cardiac troponin I hypertrophic cardiomyopathy mutation R145G in transgenic mice. J Biol Chem 283: 20484–20494.

Willott RH, Gomes AV, Chang AN, Parvatiyar MS, Pinto JR, Potter JD (2010). Mutations in Troponin that cause HCM, DCM AND RCM: what can we learn about thin filament function? J Mol Cell Cardiol 48: 882–892.

Wroblewski K, Muhandiram R, Chakrabartty A, Bennick A (2001). The molecular interaction of human salivary histatins with polyphenolic compounds. Eur J Biochem 268: 4384–4397.

Supporting information

Additional Supporting Information may be found in the online version of this article:

Figure S1 NMR spectroscopy of Ca^{2+}-cTnC-EGCg complex. Upper panel: Superposition of TROSY-type ^{15}N-^{1}H HSQC spectra of ^{15}N-labeled human Ca^{2+}-cTnC, free and in complex with EGCg. The Ca^{2+}-cTnC/EGCg ratio is 1:5. The cross-peaks of free Ca^{2+}-cTnCare shown in blue, and those of Ca^{2+}-cTnC in complex with EGCg are shown in red. Lower panel: Chemical shift perturbations due to EGCg binding to Ca^{2+}-cTnC. Horizontal solid and dotted lines show the average chemical shift throughout cTnC and standard deviation (SD), respectively. Chemical shift changes outside 2.5 SD are considered significant according to Van Selst and Jolicoeur (1994) and labelled with asterisk.
Figure S2 EGCg binding sites mapped on the crystal structure of troponin core domain complex (PDB: 1J1D) (Van Selst and Jolicoeur, 1994). The cTnIN-teminalhelix (residues 42–62) is colored cyan. The other regions of cTnIare colored blue. $cTnT_2$ is colored red. The figures were generated by PyMOL™, Molecular Graphics System, Version 0.97.

Please note: Wiley-Blackwell are not responsible for the content or functionality of any supporting materials supplied by the authors. Any queries (other than missing material) should be directed to the corresponding author for the article.

Hypertension Research (2010) 33, 748–752
© 2010 The Japanese Society of Hypertension All rights reserved 0916-9636/10 $32.00
www.nature.com/hr

ORIGINAL ARTICLE

Sex differences in the risk profile and male predominance in silent brain infarction in community-dwelling elderly subjects: the Sefuri brain MRI study

Yuki Takashima[1], Yoshikazu Miwa[2], Takahiro Mori[1], Manabu Hashimoto[1], Akira Uchino[3], Takefumi Yuzuriha[1], Toshiyuki Sasaguri[2] and Hiroshi Yao[1]

Although brain infarction is more common in men, the male predominance of silent brain infarction (SBI) was inconsistent in the earlier studies. This study was to examine the relationship between sex differences in the risk profile and SBI. We conducted a population-based, cross-sectional analysis of cardiovascular risk factors and SBI on MRI. We asked all the female participants about the age at natural menopause and parity. SBI was detected in 77 (11.3%) of 680 participants (266 men and 414 women) with a mean age of 64.5 (range 40–93) years. In the logistic analysis, age (odds ratio (OR)=2.760/10 years, 95% confidence interval (CI)=2.037–3.738), hypertension (OR=3.465, 95% CI=1.991–6.031), alcohol intake (OR=2.494, 95% CI=1.392–4.466) and smoking (OR=2.302, 95% CI=1.161–4.565) were significant factors concerning SBI. Although SBI was more prevalent among men, this sex difference disappeared on the multivariate model after adjustment for other confounders. In 215 women aged 60 years or older, age at natural menopause, early menopause, duration of menopause, number of children and age at the last parity were not significantly associated with SBI after adjustment for age. Hypertension and age were considered to be the major risk factors for SBI in community-dwelling people. Male predominance in SBI was largely due to higher prevalence of alcohol habit and smoking in men than in women in our population.
Hypertension Research (2010) **33**, 748–752; doi:10.1038/hr.2010.69; published online 30 April 2010

Keywords: asymptomatic stroke; lacunar infarction; menopause; MRI; risk factors

INTRODUCTION

Brain infarction is more common in men.[1] Male sex may be a risk factor for symptomatic stroke, whereas premenopausal women appeared to be protected from cardiovascular events or stroke. Exceptions were groups of 35–44 years and over 85 years, in which women had slightly greater stroke incidence than men.[2] Estrogen may have beneficial effects on endothelial function and atherosclerosis in addition to the hormone's effects on serum lipid concentrations, raising the possibility of sex differences in arterial remodeling.[3] The ability to have children at older age may be a marker for slow aging and extreme longevity.[4] On the contrary, Zhang *et al.*[5] have found that high gravity and high parity were associated with a higher risk of ischemic stroke. In the Framingham Heart Study, early menopause was associated with an increased incidence of ischemic stroke.[6] Taken together, female sex may be a non-modifiable protective factor against symptomatic ischemic stroke. However, the male predominance of silent brain infarction (SBI) was inconsistent in the earlier studies.[7–11]

With regard to SBI, the North Manhattan Study found that male sex was independently associated with SBI on a multivariable logistic regression model.[7] Although the Rotterdam Scan Study reported a higher prevalence of SBI among women than men, the sex difference was no longer statistically significant when adjusted for other risk factors.[8] In a population-based consecutive autopsy series of residents (the Hisayama Study), SBI tended to be more frequent (non-significant on multivariate analysis) in female among 713 subjects without clinical stroke: 16.2% of 390 men and 19.2% of 323 women with a mean age at death of 78.3 years.[9] In contrast, sex was not independently associated with an increased risk of SBI in the Cardiovascular Health Study and Framingham Offspring Study.[10,11] In this study, we conducted a population-based, cross-sectional analysis of brain MRI findings to examine the relationship between sex differences in the risk profile and SBI.

METHODS

Between 1997 and 2007, we randomly contacted approximately 1200 inhabitants aged 40 years or older, living in the rural community of Sefuri village, Saga, Japan, through the village office, and 720 subjects (60%) visited for their first MRI examination. These subjects were living independently at home

[1]Center for Emotional and Behavioral Disorders, National Hospital Organization Hizen Psychiatric Center, Saga, Japan; [2]Department of Clinical Pharmacology, Graduate School of Medical Sciences, Kyushu University, Fukuoka, Japan and [3]Department of Radiology, Saitama Medical University International Medical Center, Saitama, Japan
Correspondence: Dr H Yao, Center for Emotional and Behavioral Disorders, National Hospital Organization Hizen Psychiatric Center, Mitsu 160, Yoshinogari, Kanzaki, Saga 842-0192, Japan.
E-mail: hyao@hizen2.hosp.go.jp
Received 25 January 2010; revised 3 March 2010; accepted 17 March 2010; published online 30 April 2010

without apparent dementia. Eight subjects did not undergo MRI examination because of claustrophobia (n=5) and contraindications for MRI (n=3). Subjects with a history of stroke (n=18), brain tumor (n=5), malignant neoplasm (n=2), psychiatric disorders including depression (n=3) or a history of head trauma (n=4) were also excluded. Two cases of transient ischemic attack were included in subjects with a history of stroke: one had progressed to overt stroke 2 days later and the other proved to be a small putamenal hemorrhage on MRI. The National Hospital Organization Hizen Psychiatric Center Institutional Review Board approved the study (No. 15-1), and written informed consent was obtained from all subjects.

Participants underwent a structured clinical interview, a neurological examination, general hematology tests, biochemistry tests and ECGs. Blood pressure was measured in the sitting position by the standard cuff method after a 5-min rest. Vascular risk factors were defined as described earlier.[12,13] Briefly, arterial hypertension was considered present if a subject had a history of repeated blood pressure recordings above 140/90 mm Hg or the subject was being treated for hypertension. Diabetes mellitus was defined as fasting plasma glucose $>7.77\,mmol\,l^{-1}$ and/or HbA1c $>6.0\%$, or an earlier diagnosis of diabetes mellitus. Hyperlipidemia was defined as total serum cholesterol concentration $>5.69\,mmol\,l^{-1}$ or if the subject was being treated for hyperlipidemia. We obtained information about usual alcohol intake and type of alcohol consumed from a detailed questionnaire as described earlier.[13] We defined one drink as 10 g of ethanol, calculated as follows: 350 ml beers as 1.4 drinks, 180 ml sake (rice wine) as 2.2 drinks, 180 ml shochu (white spirits) as 3.6 drinks, 60 ml whisky as 2.0 drinks and 120 ml wine as 1.2 drinks. In this study, we defined alcohol intake as one drink or more per week, because the earlier study from the same population revealed that even light drinkers had the similar risk for SBI (odds ratio (OR)=4.1, 95% confidence interval (CI)=1.7–10.0) as moderate drinkers (OR=3.1, 95% CI=1.3–7.0). Former drinkers were considered non-drinker in this study. Smoking was defined as present if the subject smoked at least an average of 10 cigarettes per day.

We asked all the female participants about items discussed below using a questionnaire, and analyzed potential risk factors for SBI in 215 women aged 60 years or older in relation to age at natural menopause and parity. Natural menopause was considered to occur if a woman had ceased menstruating naturally for at least 1 year. Age at natural menopause was the self-reported age at last menstrual period. Early menopause was defined as natural menopause before age 40. Women were also queried as to the cause of menopause (natural, surgical, other), whether a hysterectomy was performed, number of ovaries removed, the use of hormone replacement therapy, the total number of children and the age at giving birth to her last child. Subjects with non-natural menopause were excluded from the analysis.

The combination of T1WI, T2WI and FLAIR images is required to accurately detect both SBI and white matter lesions (WMLs).[14] Therefore, T1 weighted (TR/TE=510/12 ms), T2 weighted (TR/TE=4300/110 ms) and FLAIR (TR/TI/TE=6750/1600/22 ms) images were obtained with a slice thickness of 6 mm with a 1 mm interslice gap with an MRI (1.0 T, Shimadzu Magnex XP, Kyoto, Japan). SBI was shown as low signal intensities on T1-weighted images, and their size was 5 mm or larger as described earlier (Figure 1).[12,13] We differentiated enlarged perivascular spaces from SBI on the basis of their location, shape and size.[15,16] The WMLs were defined as isointense with normal brain parenchyma on T1-weighted images, high signal intensity areas on T2-weighted images and were classified into deep white matter lesions (DWMLs) and periventricular hyperintensities (PVHs). We used the validated rating scale of DWMLs by Fazekas *et al.*[17]: Grade 0, absent; Grade 1, punctate foci; Grade 2, beginning confluence of foci; Grade 3, large confluent areas.

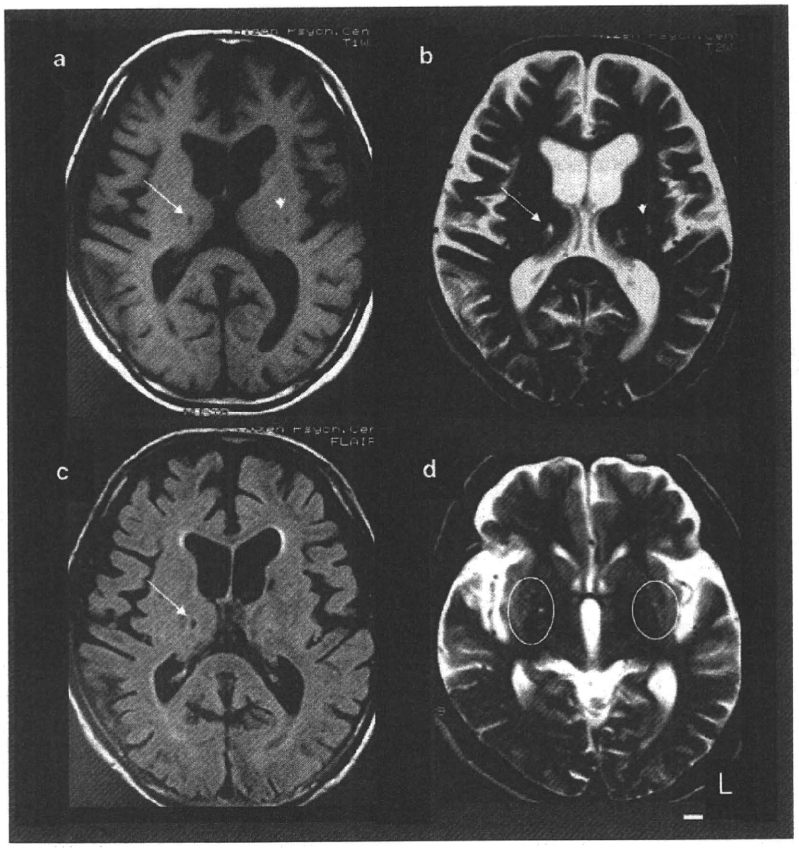

Figure 1 (**a–c**) An 80-year-old man with silent brain infarction (SBI) in the right thalamus (arrow) and the left basal ganglia (arrow head). The SBI is shown as low signal intensity on the T1 weighted (A), high signal intensity on the T2 weighted and iso or high signal intensity with or without low intensity at the center on the fluid-attenuated inversion recovery (FLAIR) images. (**d**) A 70-year-old man with dilated periventricular spaces in the bilateral lower one-third of basal ganglia (circles). Bar indicates 10 mm. L, left.

For PVHs, we determined the presence and severity (Grade 0, absent; Grade 1, pencil thin; Grade 2, smooth halo lining) using FLAIR images. All scans were reviewed independently by two authors (HY and AU) who were blinded to all clinical data. In the case of disagreement between the raters, a consensus reading was held.

All values were given as mean ± s.d. The data were analyzed with the Predictive Analysis Software (PASW Statistics 18.0, formerly called SPSS Statistics, SPSS Inc., Chicago, IL, USA). A significance level of 0.05 was used in all analyses. For the univariate analysis, the *t*-test for continuous variables, the χ^2 test for categorical variables and the non-parametric Mann–Whitney *U*-test for variables with skewed distribution were used as appropriate. We chose the variables for entry into the multivariate analysis based on the clinical and neuroradiological findings after univariate testing. Multivariate analysis was performed using the forward stepwise method of logistic analysis.

RESULTS

The subjects comprised 266 men and 414 women with a mean age of 64.5 (range 40–93) years (Table 1). SBI, DWMLs and PVHs were detected in 77 (11.3%), 204 (30.0%) and 121 (17.8%) of 680 participants, respectively. The prevalence of all these MRI findings increased steeply with age, whereas SBI alone were more frequent in men than in women (Figure 2). Of 77 subjects with SBI, 73 (95%) had only lacune(s) and 51 of 73 subjects (70%) had a single lacune.

The mean age at natural menopause was 48.7 ± 4.4 years (a median of 50 years), and the mean number of children was 3.5 ± 1.4 (a median of 3). Age at natural menopause, early menopause (10 of 215 women) and age at the last parity were not significantly associated with SBI (Table 2). Although duration of menopause (P=0.010) and number of children (P=0.052) tended to be associated with SBI on univariate analysis, these associations did not persist after adjustment for age. In this group of female subjects aged 60 years or older, alcohol habit was independently associated with SBI. Even if hypertension, diabetes mellitus and hyperlipidemia were forced into the multivariate model regardless of statistical significance, they did not affect the results of Table 2.

In the logistic analysis, age (OR=2.760/10 years, 95% CI=2.037–3.738), hypertension (OR=3.465, 95% CI=1.991–6.031), alcohol intake (OR=2.494, 95% CI=1.392–4.466) and smoking (OR=2.302, 95% CI=1.161–4.565) were significant factors concerning SBI (Table 3). Male sex was not significantly associated with WMLs. Hypertension and age, but neither alcohol nor smoking, were the major factors associated with both DWMLs and PVHs (Table 3).

Table 1 Sex differences in demographic measures

	All n=*680*	*Men* n=*266*	*Women* n=*414*
Age (years)	64.5 ± 11.5	64.3 ± 11.0	64.6 ± 11.8
Education (years)	10.1 ± 2.4	10.5 ± 2.6	9.7 ± 2.3
Body mass index (kg m^{-2})	23.0 ± 3.2	23.0 ± 3.2	22.9 ± 3.3
Hypertension (%)	38.2	37.6	38.6
Systolic blood pressure (mm Hg)	138 ± 23	135 ± 21	141 ± 24*
Diastolic blood pressure (mm Hg)	79 ± 11	81 ± 10	78 ± 11**
Mean blood pressure (mm Hg)	99 ± 13	99 ± 12	99 ± 13
Diabetes mellitus (%)	9.6	15.4	5.8**
Hyperlipidemia (%)	23.8	19.9	31.9**
Alcohol (%)	39.1	74.1	16.7**
Smoking (%)	16.3	38.7	1.9**

Values are mean ± s.d.
*P=0.002, **P<0.001 *vs.* men.

Although SBI was more prevalent among men on univariate analysis (P=0.015), this sex difference disappeared on the multivariate model after adjustment for other confounders. Age, body mass index, hypertension and blood pressure were well balanced between men and women (Table 1). Hypertension was present in 260 (38.2%) of 680 subjects. Blood pressure levels were 126 ± 16/76 ± 9, 153 ± 20/81 ± 11 and 166 ± 17/89 ± 10 mm Hg in normotensive subjects (n=420), treated hypertensive subjects (n=169) and non-treated hypertensive subjects (n=91), respectively. Common vascular risk factors such as diabetes mellitus, alcohol and smoking were more frequent in men, and more frequent hyperlipidemia in women.

DISCUSSION

This is the first study, which showed that higher prevalence of lifestyle risk factors rather than sex explains the male predominance of SBI. We found a prevalence of SBI of 11.3% in community-dwelling subjects with a mean age of 64.5 years. This is comparable with two prior studies, the Atherosclerosis Risk in Community (ARIC) Study[18] and the Framingham Heart Study[11] (prevalence and mean age: 11%, 63 years and 10.7%, 61 years, respectively). A Japanese brain check-up study, among participants who received MRI at their own expense, reported a similar prevalence of 10.6%.[19] This study showed that age, hypertension, alcohol habit and smoking were independently associated with SBI. We found a male predominance of SBI (15.0% in men *vs.* 8.9% in women), which was similar to the North Manhattan Study (21.3% in men *vs.* 15.2% in women).[7] However, male sex was not significantly associated with SBI after adjustment for other vascular risk factors. In other words, higher prevalence of risk factors such as alcohol and smoking in men produced male predominance of SBI in this study.

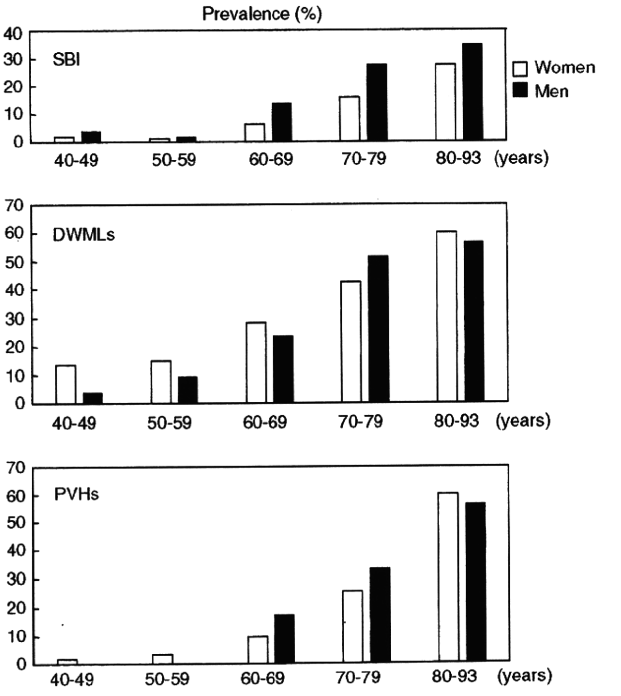

Figure 2 Prevalence of silent brain infarction (SBI), deep white matter lesions (DWMLs) and periventricular hyperintensities (PVHs) with increasing age in male and female participants.

In this study, assumed risk factors unique to women such as early menopause did not associate with SBI, and older age at the last parity, as a potential marker for longevity, seemed negative in terms of preventing SBI in women. Age at natural menopause, early menopause and age at the last parity were not significantly associated with SBI. Duration of menopause and number of children, which tended to be associated with SBI on univariate analysis, were not significant after adjustment for age. As the majority of silent infarcts are related to small vessel disease, menopause and parity might not be detected as factors relevant to SBI. Alternatively, the age at menopause and parity might be an important risk for atherosclerosis (for example large-artery occlusive infarction, carotid atherosclerosis and coronary heart disease).[20–22] Strengths of this study include that it is population based and includes a relatively large number of residents. The limitation of this study would be that we could not provide the sex differences in incidence of SBI because of the cross-sectional nature. The Rotterdam Scan Study, which reported higher prevalence of SBI among women than men,[8] showed similar SBI incidence for both sexes.[23] Sex differences in SBI incidence need to be further investigated in future studies. Another limitation of this study would be that women before age 60 were excluded from the analysis for the effects of natural menopause and parity on SBI, because SBI was rare before 60 years (2 of 139 women). Therefore, we cannot exclude the possibility that early menopause or high parity could be the basis for SBI at younger ages.

Table 2 Menopause, parity and silent brain infarction among women aged 60 years or older

	Univariate	*Multivariate*		
	P	*Odds ratio*	*95% CI*	P
Age (per 10 years)	0.004	2.573	1.395–4.746	0.002
Alcohol	0.081	3.475	1.070–11.285	0.038
Age at natural menopause	0.506			
Early menopause	0.119			
Duration of menopause (per 10 years)	0.010			
No. of children	0.052			
Age at the last parity	0.149			

Abbreviation: CI, confidence interval.

Age and hypertension are the most widely accepted risk factors for SBI, and other cardiovascular risk factors for symptomatic stroke were also found to raise the risk of SBI.[24] In the longitudinal Rotterdam Study, age, blood pressure, diabetes mellitus, cholesterol, homocysteine levels and smoking were associated with new SBI in participants without prevalent infarcts.[23] Similarly, the Framingham Offspring Study showed that atrial fibrillation, hypertension, systolic blood pressure and an elevated plasma homocysteine, but neither age nor gender were independently associated with an increased risk of SBI.[11] As most of silent infarcts are subcortical lacunar infarction, risk factors for SBI are similar to those of lacunar infarction or the small vessel disease. Recently, the community-based PATH Through Life Study showed that hypertension was the major treatable risk factor for lacunar infarcts.[25] Therefore, the present results are compatible with those reported earlier in terms of risk factor profiles of SBI.

Two earlier studies, the Cardiovascular Health Study and the ARIC Study, have investigated the effects of alcohol intake on subclinical MRI findings.[26,27] The Cardiovascular Health Study found that moderate alcohol consumption in older adults, aged 65 years or older was associated with a lower prevalence of SBI, whereas the ARIC Study showed that alcohol intake in middle-aged adults was not associated with MRI infarction. Our earlier study as well as this study revealed that even a low amount of regular drinking may be a risk factor for SBI in community-dwelling Japanese people.[13] Effects of alcohol on SBI were evident also in the selected group of female subjects with natural menopause aged 60 years or older (Table 3). Discrepancies between the results of our study and those of the earlier studies may be partly explained by racial differences such as obviously lower body mass index of Japanese compared with those of western populations, and the frequent genetic deficiency in alcohol detoxification in Japanese and Orientals.[28] Furthermore, among a Japanese population, lacunar infarction was the most common subtype of cerebral infarction,[29] whereas stroke registries of western countries have reported lower frequencies of lacunar infarction than of atherothrombotic and cardioembolic infarction. Alcohol may be partly protective against proximal segment of the cerebrovascular tree, but not for small vessels or SBI.

The relationship between smoking and SBI has been unclear. With regard to symptomatic stroke, an early meta-analysis revealed that the

Table 3 Potential risk factors for silent brain infarction and white matter lesions

	Silent brain infarction				*Deep white matter lesions*				*Periventricular hyperintensities*			
	Univariate	*Multivariate*			*Univariate*	*Multivariate*			*Univariate*	*Multivariate*		
	P	*Odds ratio*	*95% CI*	P	P	*Odds ratio*	*95% CI*	P	P	*Odds ratio*	*95% CI*	P
Age (per 10 years)	0.000	2.760	2.037–3.738	0.000	0.000	2.084	1.737–2.502	0.000	0.000	3.478	2.648–4.570	0.000
Sex (male)	0.015				NS				NS			
Hypertension	0.000	3.465	1.991–6.031	0.000	0.000	1.611	1.120–2.315	0.010	0.000	1.637	1.045–2.564	0.031
Diabetes mellitus	0.138				0.035	1.914	1.092–3.355	0.023	NS			
Hyperlipidemia	0.171				0.159				NS			
Alcohol	0.032	2.494	1.392–4.466	0.002	NS				NS			
Smoking	0.018	2.302	1.161–4.565	0.017	0.100				0.121			
Uric acid (per mg per 100 ml)	0.000				0.150				0.019	1.167	1.001–1.361	0.048

Abbreviations: CI, confidence interval; NS, non-significant.
$P>0.2$.

relative risk of stroke associated with smoking was 1.5 (95% CI= 1.4–1.6).[30] Subarachnoid hemorrhage was most clearly associated with smoking, and cerebral infarction was almost twice as likely in smokers compared with non-smokers. Although smoking may be more strongly related to atherogenic strokes rather than small vessel disease,[31] the smoking-associated increased risk was found for lacunar infarction.[32,33] Mannami *et al.*[33] summarized several plausible mechanisms for smoking-related risk of stroke such as hypercoagulable states, reduced blood flow, reduced HDL cholesterol and direct injury to endothelial cells. The ARIC Study showed that current smoking and hypertension both almost doubled the odds of SBI (1.88 for current smoking, 2.00 for hypertension).[15] In a high-risk Japanese community-dwelling population, smoking status and systolic blood pressure were independent determinant of the number of SBI.[34] This study also found an independent association of smoking with SBI. Of note, the higher prevalence of SBI in men was partly due to the fact that smoking habit in women was extremely low in our population.

In conclusion, age, hypertension, alcohol and smoking were considered to be the risk factors for SBI in community-dwelling people. We showed that higher prevalence of alcohol habit and smoking in men than in women rather than biological effects of sex resulted in apparent male predominance in SBI in our population. Therefore, modification of the lifestyle risk factors would prevent SBI particularly in men and even in women with personal habits such as alcohol consumption and cigarette smoking.

CONFLICT OF INTEREST

The authors declare no conflict of interest.

ACKNOWLEDGEMENTS

We express special thanks to T Muto and K Yamamoto for their technical assistance with the laboratory examinations and the MRI scanning, K Fukuda for valuable advice on the relationship between alcohol and SBI and N Kawahara-Ideno for registration of participants.

1 Appelros P, Stegmayr B, Terént A. Sex differences in stroke epidemiology: a systematic review. *Stroke* 2009; **40**: 1082–1090.
2 Sacco RL, Boden-Albala B, Gan R, Chen X, Kargman DE, Shea S, Paik MC, Hauser WA. Stroke incidence among white, black, and Hispanic residents of an urban community: the Northern Manhattan Stroke Study. *Am J Epidemiol* 1998; **147**: 259–268.
3 Mendelsohn ME, Karas RH. The protective effects of estrogen on the cardiovascular system. *N Engl J Med* 1999; **340**: 1801–1811.
4 Perls TT, Alpert L, Fretts RC. Middle-aged mothers live longer. *Nature* 1997; **389**: 133.
5 Zhang X, Shu XO, Gao YT, Yang G, Li H, Zheng W. Pregnancy, childrearing, and risk of stroke in Chinese women. *Stroke* 2009; **40**: 2680–2684.
6 Lisabeth LD, Beiser AS, Brown DL, Murabito JM, Kelly-Hayes M, Wolf PA. Age at natural menopause and risk of ischemic stroke: the Framingham Heart Study. *Stroke* 2009; **40**: 1044–1049.
7 Prabhakaran S, Wright CB, Yoshita M, Delapaz R, Brown T, DeCarli C, Sacco RL. Prevalence and determinants of subclinical brain infarction: the Northern Manhattan Study. *Neurology* 2008; **70**: 425–430.
8 Vermeer SE, Koudstaal PJ, Oudkerk M, Hofman A, Breteler MM. Prevalence and risk factors of silent brain infarcts in the population-based Rotterdam Scan Study. *Stroke* 2002; **33**: 21–25.
9 Shinkawa A, Ueda K, Kiyohara Y, Kato I, Sueishi K, Tsuneyoshi M, Fujishima M. Silent cerebral infarction in a community-based autopsy series in Japan. The Hisayama Study. *Stroke* 1995; **26**: 380–385.
10 Price TR, Manolio TA, Kronmal RA, Kittner SJ, Yue NC, Robbins J, Anton-Culver H, O'Leary DH. Silent brain infarction on magnetic resonance imaging and neurological abnormalities in community-dwelling older adults. The Cardiovascular Health Study. CHS Collaborative Research Group. *Stroke* 1997; **28**: 1158–1164.
11 Das RR, Seshadri S, Beiser AS, Kelly-Hayes M, Au R, Himali JJ, Kase CS, Benjamin EJ, Polak JF, O'Donnell CJ, Yoshita M, D'Agostino Sr RB, DeCarli C, Wolf PA. Prevalence and correlates of silent cerebral infarcts in the Framingham offspring study. *Stroke* 2008; **39**: 2929–2935.
12 Yao H, Takashima Y, Mori T, Uchino A, Hashimoto M, Yuzuriha T, Miwa Y, Sasaguri T. Hypertension and white matter lesions are independently associated with apathetic behavior in healthy elderly subjects: the Sefuri brain MRI study. *Hypertens Res* 2009; **32**: 586–590.
13 Fukuda K, Yuzuriha T, Kinukawa N, Murakawa R, Takashima Y, Uchino A, Ibayashi S, Iida M, Yao H, Hirano M. Alcohol intake and quantitative MRI findings among community dwelling Japanese subjects. *J Neurol Sci* 2009; **278**: 30–34.
14 Sasaki M, Hirai T, Taoka T, Higano S, Wakabayashi C, Matsusue E, Ida M. Discriminating between silent cerebral infarction and deep white matter hyperintensity using combinations of three types of magnetic resonance images: a multicenter observer performance study. *Neuroradiology* 2008; **50**: 753–758.
15 Bokura H, Kobayashi S, Yamaguchi S. Distinguishing silent lacunar infarction from enlarged Virchow-Robin spaces: a magnetic resonance imaging and pathological study. *J Neurol* 1998; **245**: 116–122.
16 Ohmine T, Miwa Y, Yao H, Yuzuriha T, Takashima Y, Uchino A, Takahashi-Yanaga F, Morimoto S, Maehara Y, Sasaguri T. Association between arterial stiffness and cerebral white matter lesions in community-dwelling elderly subjects. *Hypertens Res* 2008; **31**: 75–81.
17 Fazekas F, Kleinert R, Offenbacher H, Schmidt R, Kleinert G, Payer F, Radner H, Lechner H. Pathologic correlates of incidental MRI white matter signal hyperintensities. *Neurology* 1993; **43**: 1683–1689.
18 Howard G, Wagenknecht LE, Cai J, Cooper L, Kraut MA, Toole JF. Cigarette smoking and other risk factors for silent cerebral infarction in the general population. *Stroke* 1998; **29**: 913–917.
19 Kobayashi S, Okada K, Koide H, Bokura H, Yamaguchi S. Subcortical silent brain infarction as a risk factor for clinical stroke. *Stroke* 1997; **28**: 1932–1939.
20 ESHRE Capri Workshop Group. Hormones and cardiovascular health in women. *Hum Reprod Update* 2006; **12**: 483–497.
21 Humphries KH, Westendorp IC, Bots ML, Spinelli JJ, Carere RG, Hofman A, Witteman JC. Parity and carotid artery atherosclerosis in elderly women: the Rotterdam Study. *Stroke* 2001; **32**: 2259–2264.
22 Skilton MR, Sérusclat A, Begg LM, Moulin P, Bonnet F. Parity and carotid atherosclerosis in men and women: insights into the roles of childbearing and child-rearing. *Stroke* 2009; **40**: 1152–1157.
23 Vermeer SE, Den Heijer T, Koudstaal PJ, Oudkerk M, Hofman A, Breteler MM. Incidence and risk factors of silent brain infarcts in the population-based Rotterdam Scan Study. *Stroke* 2003; **34**: 392–396.
24 Vermeer SE, Longstreth Jr WT, Koudstaal PJ. Silent brain infarcts: a systematic review. *Lancet Neurol* 2007; **6**: 611–619.
25 Chen X, Wen W, Anstey KJ, Sachdev PS. Prevalence, incidence, and risk factors of lacunar infarcts in a community sample. *Neurology* 2009; **73**: 266–272.
26 Mukamal KJ, Longstreth Jr WT, Mittleman MA, Crum RM, Siscovick DS. Alcohol consumption and subclinical findings on magnetic resonance imaging of the brain in older adults: the cardiovascular health study. *Stroke* 2001; **32**: 1939–1946.
27 Ding J, Eigenbrodt ML, Mosley Jr TH, Hutchinson RG, Folsom AR, Harris TB, Nieto FJ. Alcohol intake and cerebral abnormalities on magnetic resonance imaging in a community-based population of middle-aged adults: the Atherosclerosis Risk in Communities (ARIC) study. *Stroke* 2004; **35**: 16–21.
28 Shibuya A, Yoshida A. Frequency of the atypical aldehyde dehydrogenase-2 gene (ALDH2(2)) in Japanese and Caucasians. *Am J Hum Genet* 1988; **43**: 741–743.
29 Tanizaki Y, Kiyohara Y, Kato I, Iwamoto H, Nakayama K, Shinohara N, Arima H, Tanaka K, Ibayashi S, Fujishima M. Incidence and risk factors for subtypes of cerebral infarction in a general population: the Hisayama study. *Stroke* 2000; **31**: 2616–2622.
30 Shinton R, Beevers G. Meta-analysis of relation between cigarette smoking and stroke. *BMJ* 1989; **298**: 789–794.
31 Mast H, Thompson JL, Lin IF, Hofmeister C, Hartmann A, Marx P, Mohr JP, Sacco RL. Cigarette smoking as a determinant of high-grade carotid artery stenosis in Hispanic, black, and white patients with stroke or transient ischemic attack. *Stroke* 1998; **29**: 908–912.
32 You R, McNeil JJ, O'Malley HM, Davis SM, Donnan GA. Risk factors for lacunar infarction syndromes. *Neurology* 1995; **45**: 1483–1487.
33 Mannami T, Iso H, Baba S, Sasaki S, Okada K, Konishi M, Tsugane S, Japan Public Health Center-Based Prospective Study on Cancer and Cardiovascular Disease Group. Cigarette smoking and risk of stroke and its subtypes among middle-aged Japanese men and women: the JPHC Study Cohort I. *Stroke* 2004; **35**: 1248–1253.
34 Eguchi K, Kario K, Hoshide S, Hoshide Y, Ishikawa J, Morinari M, Hashimoto T, Shimada K. Smoking is associated with silent cerebrovascular disease in a high-risk Japanese community-dwelling population. *Hypertens Res* 2004; **27**: 747–754.

Yoshihara et al. Molecular Cancer 2010, 9:245
http://www.molecular-cancer.com/content/9/1/245

MOLECULAR CANCER

RESEARCH Open Access

Anti-angiogenic effects of differentiation-inducing factor-1 involving VEGFR-2 expression inhibition independent of the Wnt/β-catenin signaling pathway

Tatsuya Yoshihara[1,2], Fumi Takahashi-Yanaga[1*], Fumie Shiraishi[1], Sachio Morimoto[1], Yutaka Watanabe[3], Masato Hirata[4], Sumio Hoka[2], Toshiyuki Sasaguri[1]

Abstract

Background: Differentiation-inducing factor-1 (DIF-1) is a putative morphogen that induces cell differentiation in *Dictyostelium discoideum*. DIF-1 inhibits proliferation of various mammalian tumor cells by suppressing the canonical Wnt/β-catenin signaling pathway. To assess the potential of a novel cancer chemotherapy based on the pharmacological effect of DIF-1, we investigated whether DIF-1 exhibits anti-angiogenic effects *in vitro* and *in vivo*.

Results: DIF-1 not only inhibited the proliferation of human umbilical vein endothelial cells (HUVECs) by restricting cell cycle in the G_0/G_1 phase and degrading cyclin D1, but also inhibited the ability of HUVECs to form capillaries and migrate. Moreover, DIF-1 suppressed VEGF- and cancer cell-induced neovascularization in Matrigel plugs injected subcutaneously to murine flank. Subsequently, we attempted to identify the mechanism behind the anti-angiogenic effects of DIF-1. We showed that DIF-1 strongly decreased vascular endothelial growth factor receptor-2 (VEGFR-2) expression in HUVECs by inhibiting the promoter activity of human VEGFR-2 gene, though it was not caused by inhibition of the Wnt/β-catenin signaling pathway.

Conclusion: These results suggested that DIF-1 inhibits angiogenesis both *in vitro* and *in vivo*, and reduction of VEGFR-2 expression is involved in the mechanism. A novel anti-cancer drug that inhibits neovascularization and tumor growth may be developed by successful elucidation of the target molecules for DIF-1 in the future.

Background

Angiogenesis is a multi-step process essential for tumor growth and metastasis, which involves endothelial cell proliferation, migration and capillary formation [1-4]. Among many soluble and matrix-derived angiogenic growth factors and regulators of angiogenesis involved in neovascularization, vascular endothelial growth factor (VEGF) plays a crucial role in the proliferation, migration and survival of vascular endothelial cells [2,5-7].

The VEGF family consists of six members, VEGF-A, VEGF-B, VEGF-C, VEGF-D, VEGF-E and the placenta growth factor (PLGF) [4,7,8]. Among them, VEGF-A is known as the most important factor for many angiogenic processes. VEGF-A binds to two tyrosine kinase receptors, VEGFR-1 (Flt-1) and VEGFR-2 (KDR/Flk-1) [2,8-11]. Signaling through VEGFR-1 is related to embryonic angiogenesis and acts as a regulator of VEGFR-2 [7,8,12,13]. Although the affinity of VEGFR-2 for VEGF is lower than that of VEGFR-1, VEGFR-2 is more potent than VEGFR-1 in stimulating endothelial cell proliferation and migration [11,14]. VEGFR-2 expression is almost restricted to vascular endothelial cells and it has been reported that VEGFR-2 expression was markedly up-regulated during chronic inflammation, wound repair and tumor growth [5,15,16].

Differentiation-inducing factors (DIFs) were identified in *Dictyostelium discoideum* as morphogens required for stalk cell differentiation [17]. In the DIF family, DIF-1 (1-(3, 5-dichloro-2, 6-dihydroxy-4-methoxyphenyl)-1-hexanone) was the first to be identified. The actions of

* Correspondence: yanaga@clipharm.med.kyushu-u.ac.jp
[1]Department of Clinical Pharmacology, Faculty of Medical Sciences, Kyushu University, Fukuoka 812-8582, Japan
Full list of author information is available at the end of the article

BioMed Central

© 2010 Yoshihara et al; licensee BioMed Central Ltd. This is an Open Access article distributed under the terms of the Creative Commons Attribution License (http://creativecommons.org/licenses/by/2.0), which permits unrestricted use, distribution, and reproduction in any medium, provided the original work is properly cited.

DIFs are not limited to *Dictyostelium* and they strongly inhibit the proliferation of human cells [18,19]. Previously, we reported that DIFs inhibited the Wnt/β-catenin signaling pathway via glycogen synthase kinase-3β (GSK-3β) activation, leading to cell cycle arrest at G_0/G_1 phase through suppression of cyclin D1 expression in various human tumor cells [20-23]. It is well known that the Wnt/β-catenin signaling pathway plays a number of key roles in embryonic development and maintenance of homeostasis in matured tissues. And also, this signaling pathway has been reported to play important roles in the proliferation and migration of endothelial cells, resulting in the promotion of angiogenesis [24-28].

In this study, we investigated the effect of DIF-1 on angiogenesis in *in vitro* and *in vivo* systems. We revealed that DIF-1 decreased the expression of VEGFR-2 in protein and mRNA levels via the suppression of the promoter activity by a Wnt/β-catenin signaling pathway-independent mechanism. Our results suggest that the suppression of VEGFR-2 expression could be one mechanism of the inhibition of angiogenesis induced by DIF-1 and that DIF-1 suppressed not only the Wnt/β-catenin signaling pathway but also neovascularization.

Results

DIF-1 inhibited HUVEC proliferation

DIF-1 exhibits powerful anti-proliferative effects in various mammalian cells [18-23] and we previously reported that DIF-3 induced cell cycle arrest by reducing cyclin D1 in HUVECs [20]. In this present study, we first examined whether DIF-1 also inhibited HUVEC proliferation. As shown in Figure 1A, DIF-1 strongly inhibited HUVEC proliferation in a dose-dependent manner. This anti-proliferative effect was unlikely to be caused by cytotoxicity, because the number of dead cells indicated by the trypan blue exclusion test was not increased by treatment with DIF-1 (data not shown). We next examined the effects of DIF-1 on cell cycle distribution using flow cytometry. As shown in Figure 1B, the cell population in the G_0/G_1 phase significantly increased and the population in S and G_2/M phases decreased, indicating that DIF-1 induced G_0/G_1 arrest in HUVECs. These results were consistent with that published in our previous reports [19-21].

DIF-1 induced proteolysis of cyclin D1 in HUVECs

We previously reported that DIF-1 had strong effects on cyclin D1 protein level [21,22]. Therefore, we examined the effects of DIF-1 on cyclin D1 protein quantity using HUVECs. DIF-1 rapidly reduced the protein level of cyclin D1 in time- and dose-dependent manners (Figure 2A and 2B, respectively). Next, we examined the effects of proteasome inhibitor MG132, since cyclin D1 has been reported to be degraded by ubiquitin-dependent proteolysis. MG132 significantly attenuated the effects of DIF-1, indicating that DIF-1 induced proteolysis of cyclin D1 in HUVECs (Figure 2C).

DIF-1 inhibited angiogenesis *in vitro*

To evaluate the effects of DIF-1 on angiogenesis *in vitro*, we performed tube formation assay. HUVECs formed blood vessel-like structure (tubes) on Matrigel-coated wells following incubation for 8 h. However, DIF-1-treated HUVECs almost failed to form vessel-like structures and the number of areas surrounded by tubes was significantly smaller than that in control cells (Figure 3A). Subsequently, the effects of DIF-1 on HUVECs migration were evaluated using a Boyden Chamber. Although the cells migrated into the lower chamber even in the absence of VEGF, the number of migrating cells increased by about 30% when VEGF was added to the lower chamber. Therefore, VEGF was added to the lower chamber when the effect of DIF-1 was investigated. Although VEGF in the lower chamber induced cell migration after incubation for 10 h, DIF-1 significantly reduced the number of migrated cells (Figure 3B). These results clearly indicated that DIF-1 inhibited angiogenesis *in vitro*.

DIF-1 inhibited angiogenesis *in vivo*

We examined the effects of DIF-1 on angiogenesis *in vivo* by Matrigel plug assay. VEGF containing-Matrigel was prepared with or without DIF-1 (30 μM) and injected into the flanks of mice. As shown in Figure 4, blood vessels indicated by the expression of PECAM-1/CD31, an endothelial cell-specific antigen, were strongly induced into the injected Matrigel plugs. On the other hand, the level of PECAM-1/CD31 expression was significantly lower in DIF-1-containing Matrigel plugs than in the control plugs, indicating the presence of fewer blood vessels.

Subsequently, we examined the effects of DIF-1 on tumor-induced angiogenesis using HeLa cells. Two weeks after injection, Matirgel/HeLa cell mixture formed tumor mass and blood vessels were grown into the mass. Immunohistochemical analysis of PECAM-1/CD31 in tumor masses clearly showed that the content of blood vessels was much less in DIF-1-containing masses (Figure 5A-I). This finding was also confirmed by Western blot analysis. As shown in Figure 5J, the level of PECAM-1/CD31 expression was significantly lower in DIF-1-containing masses than in the control masses. These results indicated that DIF-1 inhibited blood vessel growth induced by VEGF and tumor cells.

DIF-1 decreased VEGFR-1 and VEGFR-2 protein expression

It is well known that VEGF-A, a major regulator for angiogenesis, binds to VEGFR-1 (Flt-1) and VEGFR-2

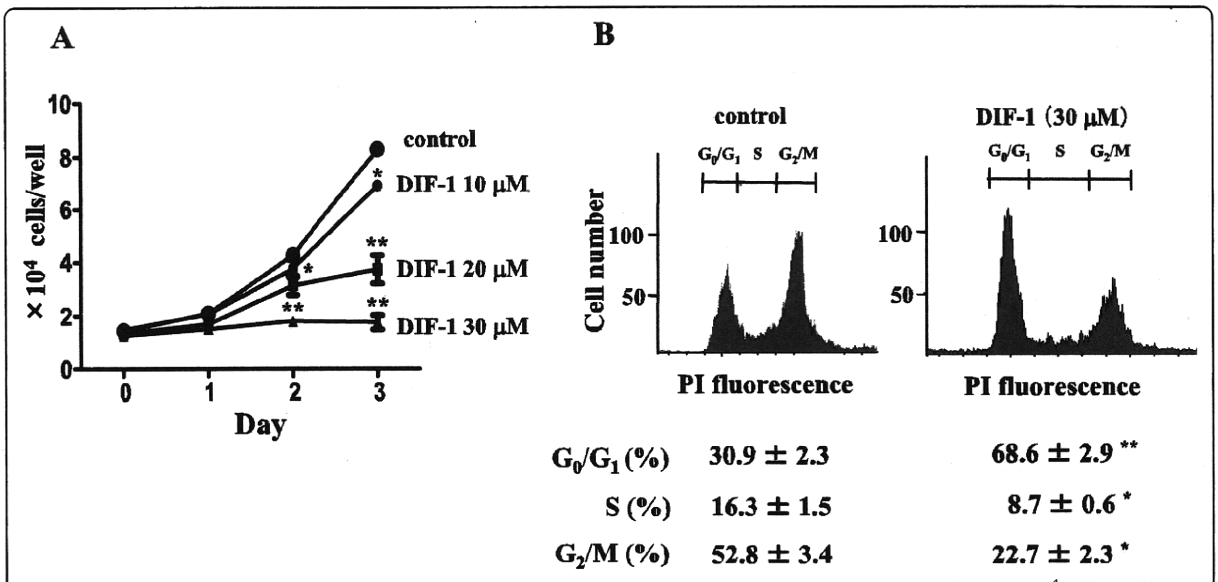

Figure 1 DIF-1 inhibited HUVECs proliferation. (A) Cell proliferation assay. HUVECs seeded on a 24-well plate (1.0×10^4 cells/well) were incubated with various amount of DIF-1. Cells were harvested by trypsin/EDTA treatment at the times indicated and enumerated. Values are mean ± SE of three independent experiments and statistically analyzed using a one-way ANOVA with Bonferroni post-hoc test. The asterisk indicates *P < 0.05 and **P < 0.01 versus control. (B) Flow cytometry. HUVECs were incubated with DIF-1 (30 μM) for 24 h and then harvested by the trypsin/EDTA treatment. Cells were stained with propidium iodide (PI) and fluorescence of nuclei was measured. The percentages of cell number in the cell cycle phases are also shown. The results are means ± SE of three independent experiments. The asterisk indicates *P < 0.01 and **P < 0.001 versus control.

(KDR/Flk-1) to transduce its signal. To clarify the mechanism by which DIF-1 suppresses angiogenesis, first we examined the effects of DIF-1 on VEGFR-1 and VEGFR-2 expression in HUVECs by Western blot analysis. As shown in Figure 6A, although DIF-1 significantly reduced the expression of both receptors in HUVECs, the effect was much stronger in VEGFR-2 than VEGFR-1.

VEGF increases VEGFR-2 phosphorylation on Tyr^{1175} for activation [29-31]. Although DIF-1 decreased the phosphorylation level of Tyr^{1175} on VEGFR-2 in a time-dependent manner, it was parallel with the time course of the VEGFR-2 protein amount, indicating that DIF-1 had no significant effects on the level of VEGFR-2 phosphorylation (Figure 6B).

DIF-1 reduced VEGFR-2 protein synthesis

To clarify the mechanism of DIF-1-induced VEGFR-2 protein suppression, we first examined the effects of DIF-1 on VEGFR-2 degradation using protein synthesis inhibitor cycloheximide. As shown in Figure 7A, DIF-1 did not accelerate reduction in VEGFR-2 protein quantity, indicating that DIF-1 had no significant effects on VEGFR-2 proteolysis.

Next, we investigated VEGFR-2 protein synthesis. HUVECs were pretreated with cycloheximide for 3 h and then the medium was changed to fresh growth medium to wash out cycloheximide. As shown in Figure 7B, after VEGFR-2 protein disappeared following cycloheximide treatment, it was rapidly restored and reached a plateau after 1 h incubation. However, restoration of VEGFR-2 protein was significantly delayed by DIF-1 treatment.

DIF-1 suppressed VEGFR-2 mRNA level and VEGFR-2 promoter activity

Subsequently, we examined the effect of DIF-1 on the mRNA expression of VEGFR-2 in HUVECs by real-time PCR analysis and found that DIF-1 significantly suppressed VEGFR-2 mRNA level (Figure 8A). We further examined the effects of DIF-1 on human VEGFR-2 gene promoter activity using a luciferase reporter plasmid. Since the efficiency of DNA transfection in HUVECs was low (10% to 20%), we also employed BAECs in which transfection efficiency was much higher (60% to 70%) [32]. As shown in Figure 8B and 8C, luciferase reporter activity driven by the 5'-flanking region of human VEGFR-2 gene in HUVECs (B) or BAECs (C) was increased as incubation proceeded. However, the promoter activity was not significantly increased in DIF-1-treated HUVECs and BAECs. Therefore DIF-1 appeared to suppress VEGFR-2 protein and mRNA expressions by inhibiting the promoter activity in HUVECs.

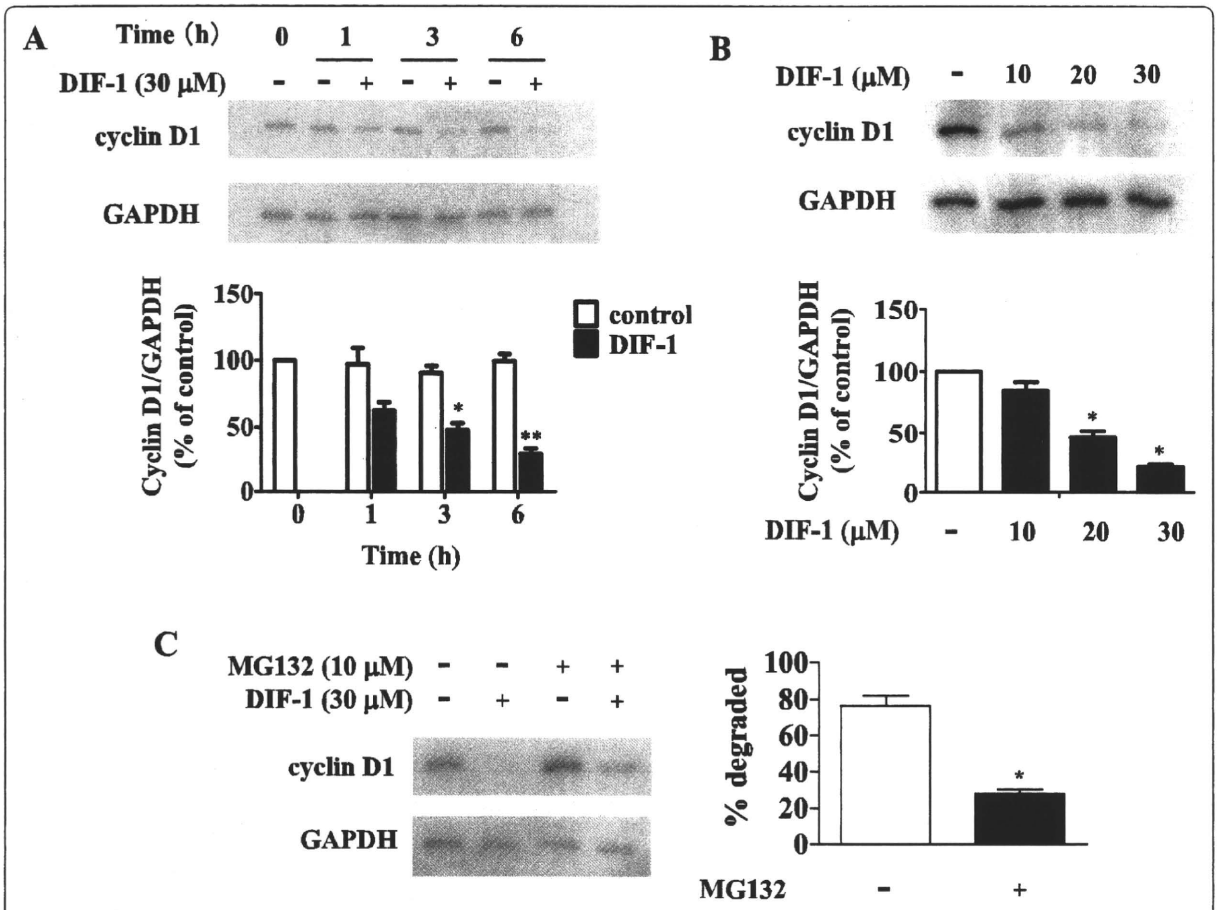

Figure 2 The effect of DIF-1 on cyclin D1 protein amount. (A) Time-course. HUVECs were incubated with or without DIF-1 (30 μM) for the periods indicated. Samples were subjected to Western blot analysis using the anti-cyclin D1 antibody. The membrane was re-probed with the anti-GAPDH antibody. The levels of protein bands were quantified and shown as percentages of the control level at time 0. Values are mean ± SE of three independent experiments. The asterisk indicates *P < 0.01 and **P < 0.001 versus control. (B) Dose dependency. HUVECs were incubated with or without various amount of DIF-1 for 4 h. Samples were subjected to Western blot analysis using the anti-cyclin D1 antibody. The membrane was re-probed with the anti-GAPDH antibody. The levels of protein bands were quantified and shown as percentages of the control level. Values are mean ± SE of three independent experiments. The asterisk indicates *P < 0.001 versus control. (C) Effect of MG132. HUVECs were pretreated with MG132 (10 μM) for 3 h and incubated with or without DIF-1 (30 μM) for 6 h. Samples were subjected to Western blot analysis using the anti-cyclin D1 antibody and the membrane was re-probed with the anti-GAPDH antibody. The levels of protein bands are quantified and shown as percentages of the degraded amounts. Values are mean ± SE of three independent experiments. The asterisk indicates *P < 0.01 and versus control.

Wnt-3a suppressed VEGFR-2 promoter activity

As previously reported, DIF-1 suppressed the Wnt/β-catenin signaling pathway by activating GSK-3β in tumor cells. Moreover, the Wnt/β-catenin signaling pathway has been shown to play an important role in promoting angiogenesis. Therefore, we examined the involvement of the Wnt/β-catenin signaling pathway in DIF-1-induced VEGFR-2 suppression. As shown in Figure 9A, DIF-1 significantly inhibited TOPflash (TCF reporter plasmid) activity, whereas it did not affect FOPflash (negative control) activity. Furthermore, as shown in Figure 9B, DIF-1 reduced the phosphorylation level of Ser^9 on GSK-3β, indicating that DIF-1 certainly inhibited the Wnt/β-catenin signaling pathway by activating GSK-3β in HUVECs.

Although VEGF is one of the target genes of the Wnt/β-catenin signaling pathway [33,34], it has not been elucidated whether VEGFR-2 gene also belongs to the target genes of this signaling pathway. Therefore, the effects of Wnt3a as an activator of the Wnt/β-catenin signaling pathway on VEGFR-2 protein expression were examined. Although the amount of VEGFR-2 protein was increased after a 24 h-incubation period, treatment with Wnt3a suppressed VEGFR-2 protein increase (Figure 10A). This observation was confirmed by the luciferase reporter assay using the 5'-flanking region of

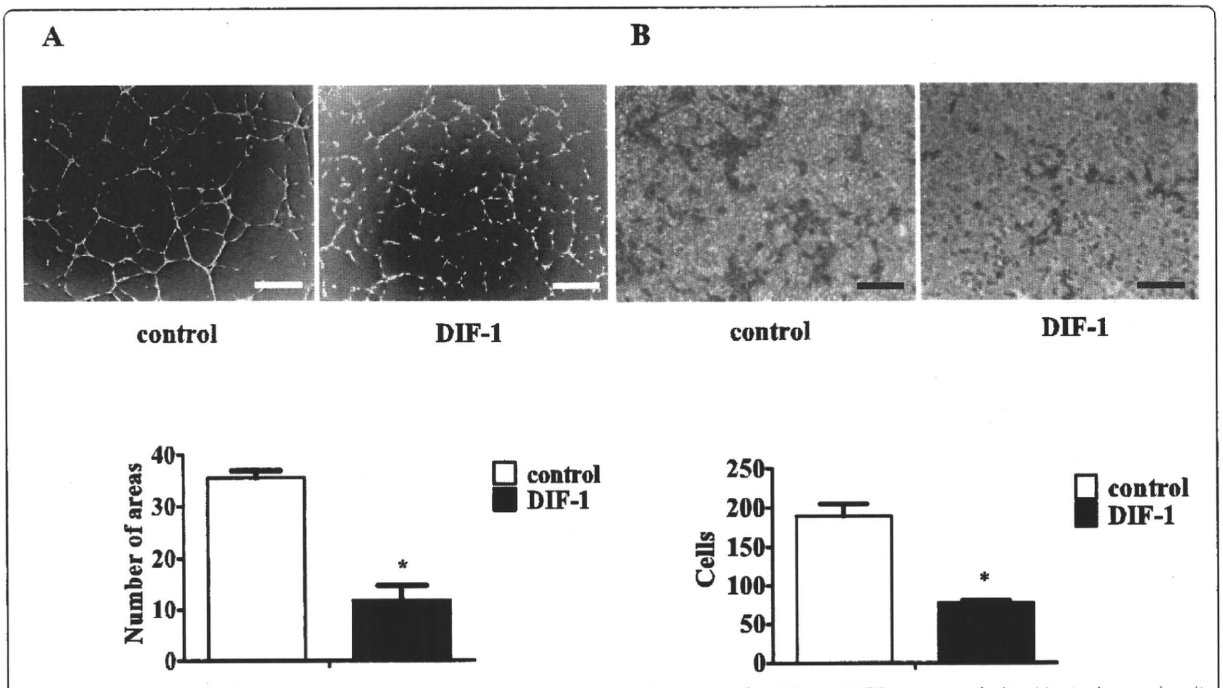

Figure 3 DIF-1 inhibited *in vitro* angiogenesis. (A) DIF-1 inhibited tube formation of HUVECs. HUVECs were seeded in Matrigel-coated well with or without DIF-1 30 μM and incubated for 8 h. The tube formation of control HUVECs was normalized as 100%. Each value represents the mean ± SE of three independent experiments. The asterisk indicates *P < 0.01 versus control. The scale bars indicate 200 μm. (B) DIF-1 inhibited the migration of HUVECs. HUVECs were seeded into the upper part of Boyden chamber. The lower compartments were filled with 600 μl of DMEM supplemented with 0.1% bovine serum albumin and 20 ng/ml (0.52 nM) VEGF. After HUVECs were incubated for 10 h, the migrated cells on the lower surface of the membrane were quantified by counting the number of cells in ten random fields per membrane and expressed as cells/fields (mean ± SE). Data are representative of three other experiments. The asterisk indicates *P < 0.01 versus control. The scale bars indicate 500 μm.

the human VEGFR-2 gene. As shown in Figure 10B, Wnt3a suppressed VEGFR-2 promoter activity slightly but significantly in HUVECs, whereas it clearly increased TOPflash activity. These results indicated that Wnt3a suppressed VEGFR-2 expression via inhibition of promoter activity, suggesting that VEGFR-2 gene expression was suppressed by activating the Wnt/β-catenin signaling pathway.

Taken together, although DIF-1 suppressed the Wnt/β-catenin signaling pathway in HUVECs as well as tumor cells, inhibition of VEGFR-2 promoter activity induced by DIF-1 was not due to suppression of this signaling pathway.

Discussion

In this study, we demonstrated that DIF-1 strongly inhibited angiogenesis *in vitro* and *in vivo*. As it is known that VEGF-A signal plays a prominent role in angiogenesis, we paid special attention to two types of VEGF receptors, VEGFR-1 and VEGFR-2. Although DIF-1 decreased the levels of protein expression of both receptors on HUVECs, the effects were faster and stronger in VEGFR-2 than VEGFR-1. Activation of VEGFR-2 by VEGF-A depends on the phosphorylation status of several tyrosine residues (such as 951, 1059, 1175, and 1214) in VEGFR-2. Among these tyrosine residues, Tyr^{1175} is the binding site of phospholipase-Cγ, a main signal transducer of VEGFR-2 [32-34]. However, as shown in Figure 6B, DIF-1 did not have significant effects on the Tyr^{1175} phosphorylation status, suggesting that DIF-1 did not affect VEGFR-2 activation. Since VEGFR-2 is a direct signal transducer for pathological angiogenesis as observed in cancers, the powerful reduction of VEGFR-2 protein levels may be involved in DIF-1 induced anti-angiogenic effects.

We also attempted to clarify the mechanism by which DIF-1 reduced the amount of VEGFR-2 protein. DIF-1 affected the synthesis rather than proteolysis of VEGFR-2. This was consistent with the result that DIF-1 inhibited the mRNA expression and promoter activity of VEGFR-2. However, degrees of suppression of the mRNA expression (29%) and promoter activity (24%) were relatively small compared to VEGFR-2 protein quantity suppression (93%) after 24 h-treatment with DIF-1. The same sort of phenomenon was also observed by Wnt3a (16% promoter activity suppression vs. 34%

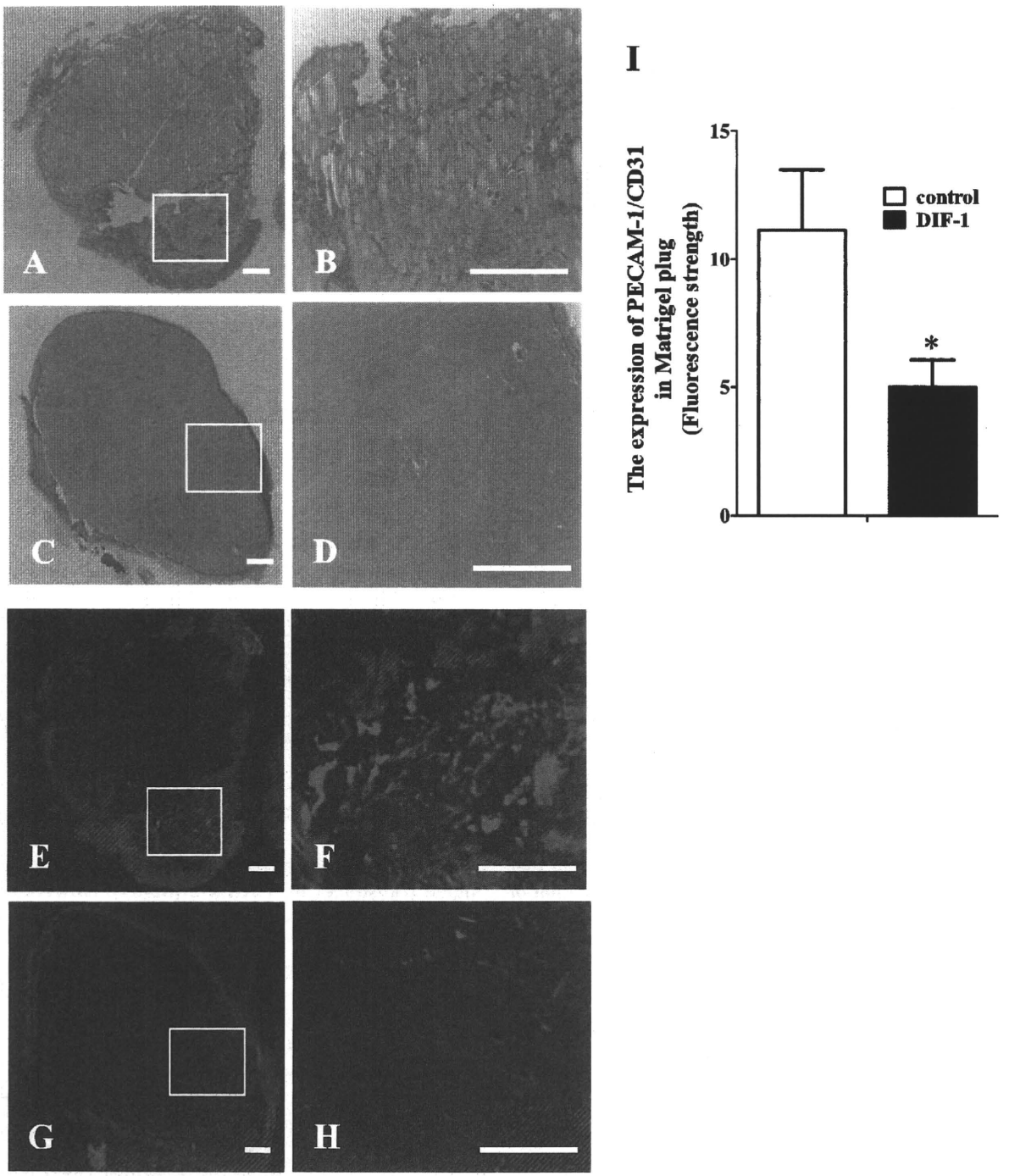

Figure 4 DIF-1 suppressed VEGF-induced angiogenesis in Matrigel plug. VEGF-containing Matrigel was injected subcutaneously into the flanks of 6-week old C57/BL6 mice. Seven days later, Matrigel plug was extracted and embedded in paraffin. Sections were stained with hematoxylin-eosin staining (A-D) and immunofluorescence staining using PECAM-1(CD31) (E-H) (Higher magnification of the boxed areas in A, C, E and G are shown in B, D, F and H, respectively). The scale bars indicate 500 μm. (I) The expression of PECAM-1 (CD31) was analyzed with fluorescence microscopy and expressed as the strength of fluorescence in Matrigel-plug (mean ± SE) of three independent experiments. The asterisk indicates *$P < 0.05$ versus control.

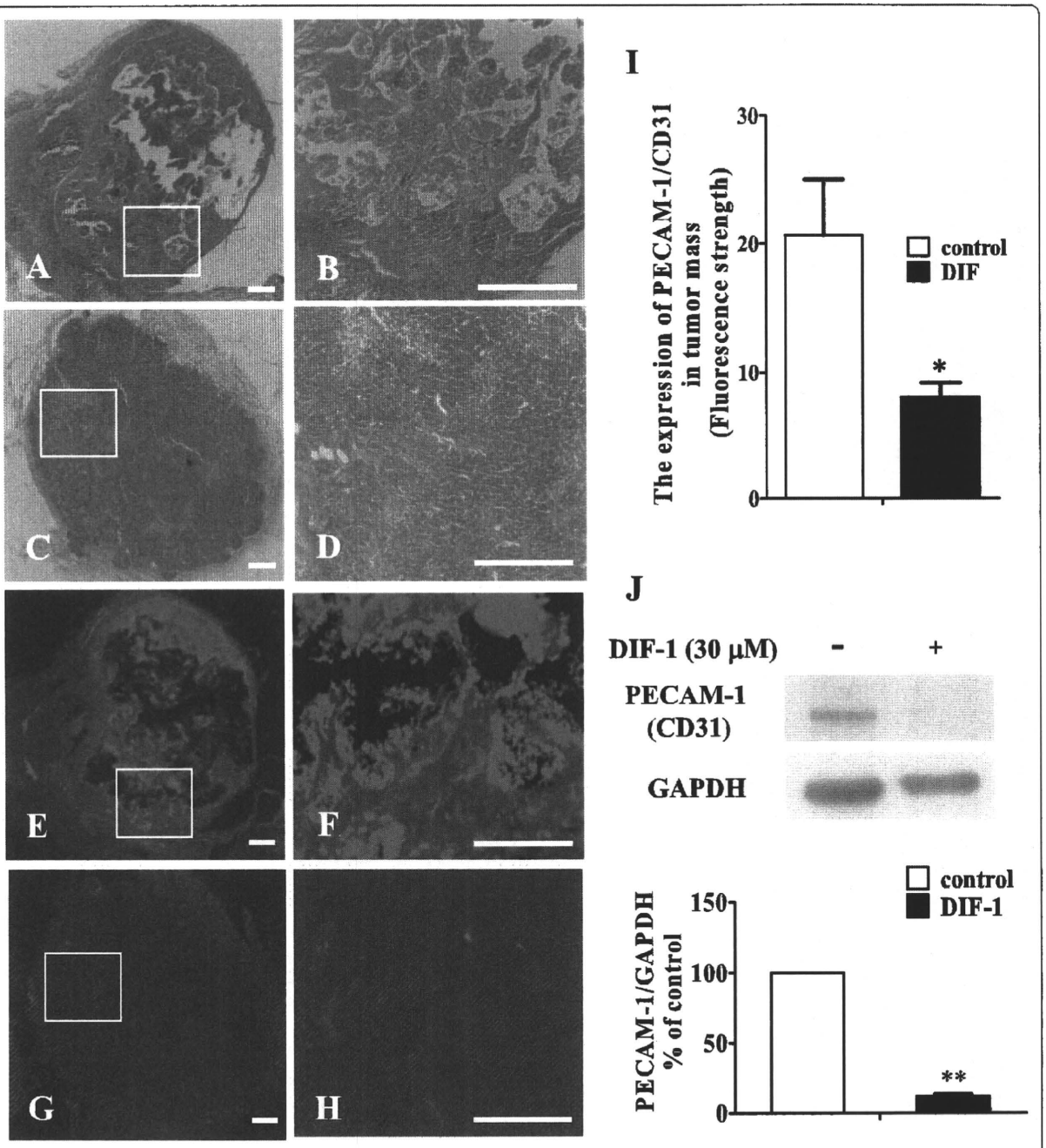

Figure 5 DIF-1 inhibited angiogenesis in xenograft tumor. (A-I) DIF-1 suppressed human cervical carcinoma cell line (HeLa)-induced angiogenesis. HeLa cells mixed with liquid Matrigel in the presence or absence of 30 μM of DIF-1 were injected subcutaneously into the flanks of nude mice. The removed tumor sections were stained with hematoxylin-eosin staining (A-D) and immunofluorescence staining using PECAM-1(CD31) (E-H) (Higher magnification of the boxed areas in A, C, E and G are shown in B, D, F and H, respectively). The scale bars indicate 500 μm. (I) The expression of PECAM-1 (CD31) was analyzed with fluorescence microscopy and expressed as the mean strength of fluorescence in Matrigel-plug (mean ± SE) of three independent experiments. (J) DIF-1 suppressed PECAM-1 protein expression in the removed tumors. The samples of the removed tumor were subjected to Western blot analysis using the anti-PECAM-1 (CD31) antibody. The membrane was re-probed with the anti-GAPDH antibody. The levels of protein bands were quantified and are shown as percentage of the control level. Values are mean ± SE of three independent experiments. The asterisk indicates *$P < 0.05$, **$P < 0.001$ versus control.